JCI The Journal of Clinical Investigation

Absence of intracellular lipolytic inhibitor G0S2 enhances intravascular triglyceride clearance and abolishes diet-induced hypertriglyceridemia

Yongbin Chen, … , Cailin E. McMahon, Jun Liu

J Clin Invest. 2025. https://doi.org/10.1172/JCI181754.

Research In-Press Preview **Endocrinology** **Metabolism**

Graphical abstract

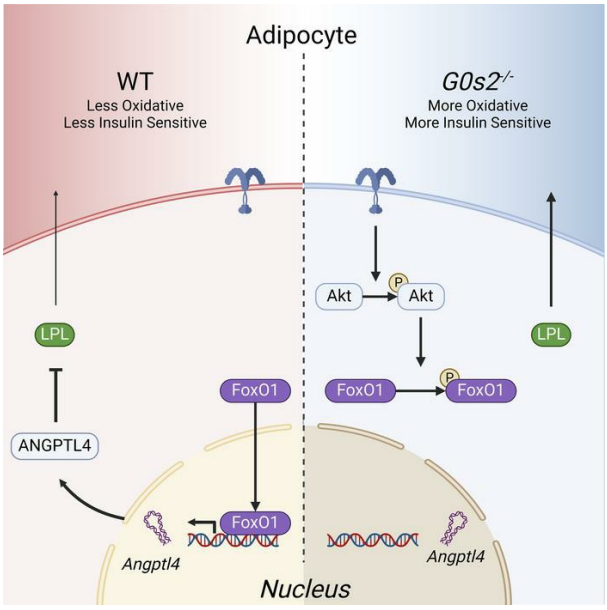

Absence of intracellular lipolytic inhibitor G0S2 enhances intravascular triglyceride clearance and abolishes diet-induced hypertriglyceridemia

Yongbin Chen[1], Scott M. Johnson[2], Stephanie D. Burr[1,3], Davide Povero[1,4], Aaron M. Anderson[5], Cailin E. McMahon[1,6], and Jun Liu[1,3,*]

[1] Department of Biochemistry and Molecular Biology; Mayo Clinic College of Medicine & Science; Rochester, MN, 55905; USA.

[2] Department of Cell Biology; University of Texas Southwestern Medical Center; Dallas, TX, 75390; USA.

[3] Division of Endocrinology, Diabetes, Metabolism and Nutrition; Mayo Clinic in Rochester; Rochester, MN, 55905; USA.

[4] Division of Gastroenterology and Hepatology; Mayo Clinic in Rochester; Rochester, MN, 55905; USA.

[5] Department of Developmental Biology, Washington University School of Medicine in St. Louis, St. Louis, Missouri 63110, USA.

[6] Molecular Biology and Genetics Department; Cornell College of Agriculture and Life Sciences; Ithaca, NY, 14853; USA.

***Correspondence:** Jun Liu, Guggenheim Building 14-11A, 222 3rd Avenue SW, Rochester, MN 55905. Phone: 507-284-8120; Email: liu.jun@mayo.edu

Conflict of Interest: The authors have declared that no conflict of interest exists.

Keywords: lipolysis, lipase, triglyceride, hypertriglyceridemia, atherosclerosis, inhibitor, LDL receptor, ATGL, LPL, ANGPTL4, G0S2, insulin.

Summary Statement: We define the role of intracellular lipolytic inhibitor G0S2 in adipose tissue in the regulation of intravascular lipolysis and development of diet-induced hypertriglyceridemia and atherosclerosis.

Abstract

The interplay between intracellular and intravascular lipolysis is crucial for maintaining circulating lipid levels and systemic energy homeostasis. Adipose triglyceride lipase (ATGL) and lipoprotein lipase (LPL), the primary triglyceride (TG) lipases responsible for these two spatially separate processes, are highly expressed in adipose tissue. Yet, their coordinated regulation remains undetermined. Here, we demonstrate that genetic ablation of G0S2, a specific inhibitory protein of ATGL, completely abolishes diet-induced hypertriglyceridemia and significantly attenuates atherogenesis in mice. These effects are attributed to enhanced whole-body TG clearance, not altered hepatic TG secretion. Specifically, G0S2 deletion increases circulating LPL concentration and activity, predominantly through LPL production from white adipose tissue (WAT). Strikingly, transplantation of G0S2-deficient WAT normalizes plasma TG levels in mice with hypertriglyceridemia. In conjunction with improved insulin sensitivity and decreased ANGPTL4 expression, the absence of G0S2 enhances the stability of LPL protein in adipocytes, a phenomenon that can be reversed upon ATGL inhibition. Collectively, these findings highlight the pivotal role of adipocyte G0S2 in regulating both intracellular and intravascular lipolysis, and the possibility of targeting G0S2 as a viable pharmacological approach to reduce circulating TGs.

Introduction

Triglycerides (TGs) represent the largest energy reservoir in the body. White adipose tissue (WAT), the primary TG storage depot, is a dynamic and metabolically active organ that significantly contributes to whole-body lipid and energy homeostasis (1, 2). Upon feeding, adipocytes secrete lipoprotein lipase (LPL), which is involved in the hydrolytic breakdown of circulating TGs into free fatty acids (FAs) and glycerol. Free FAs are subsequently taken up by adipocytes and esterified to form new TGs for storage in intracellular lipid droplets (3, 4). In response to fasting or extended exercise, these TGs are hydrolyzed through the sequential action of adipose triglyceride lipase (ATGL) and hormone-sensitive lipase (HSL), resulting in the release of free FAs and glycerol for utilization by other tissues (5, 6). Thus, TG turnover in adipose tissue is largely mediated by intravascular and intracellular lipolysis through the action of LPL and ATGL. However, the coordinated regulation of these two spatially separate processes remains poorly understood.

LPL is the principal player in the clearance of circulating TG-rich lipoproteins (TRLs) such as chylomicrons and very-low-density lipoproteins (VLDL) and their remnants. TRLs are arrested at the capillary endothelium by LPL, which forms a complex with glycosylphosphatidylinositol-anchored high-density lipoprotein-binding protein 1 (GPIHBP1) (7). The importance of LPL and GPIHBP1 for plasma TG catabolism in humans is evidenced by the fact that a genetic deficiency in either protein causes a condition of hypertriglyceridemia known as familial chylomicronemia syndrome (FCS) (8). Similarly, mice deficient in LPL or GPIHBP1 are severely hypertriglyceridemic (9, 10). As elevated plasma TGs are known to be associated with an

increased risk of atherosclerotic cardiovascular disease (ASCVD), LPL is generally viewed as an antiatherogenic enzyme (11). However, existing evidence suggests a role of LPL expressed by macrophages in the vessel wall in promoting lipid uptake and foam cell formation (12, 13). Thus, there is a great need to understand the tissue-specific regulation and contribution of LPL to hypertriglyceridemia and atherosclerosis.

The ANGPTL (angiopoietin-like) family of proteins, particularly ANGPTL3, ANGPTL4, and ANGPTL8, act as endogenous antagonists of LPL (14). They are involved in the tissue-specific regulation of LPL under various physiological conditions. In WAT, fasting induces the expression of ANGPTL4, thereby downregulating LPL activity and directing circulating TGs towards oxidative tissues (15-17). Several mechanisms have been proposed to underlie LPL modulation by ANGPTL4 (18, 19). Apart from directly binding and inhibiting LPL extracellularly, ANGPTL4 has been shown to promote intracellular cleavage of LPL in the post-endoplasmic reticulum (ER) compartment via proprotein convertase subtilisin/kexin type 3 (PCSK3), leading to subsequent LPL degradation in adipocytes (20, 21). Genetic ablation of *Angptl4* either globally or specifically in adipose tissue results in enhanced LPL activity, rapid clearance of circulating TGs, and reduced ectopic lipid deposition in liver and muscle (15, 17). This aligns with the observation that ANGPTL4 expression is most abundant in adipose tissue (15-17). The ablation of *Angptl4* in adipose tissue also promotes the clearance of proatherogenic lipoproteins, reduces inflammation, and mitigates atherosclerosis (22). These findings bolster the potential of focusing on neutralizing ANGPTL4 to prevent both hypertriglyceridemia and atherogenesis (23, 24).

ATGL is the rate-limiting enzyme that catalyzes the first step of intracellular lipolysis, converting TG to diacylglycerol (DG) and one free FA (6, 25). Previous research conducted by our laboratory and others has established a small protein encoded by the g0/g1 switch gene 2 (G0S2) as a potent endogenous inhibitor of ATGL (26-29). Subsequent animal studies have provided compelling evidence demonstrating the role of G0S2 as a major metabolic and energy regulator in adipose tissue, liver, and cardiac muscle through its inhibitory action on ATGL (27, 30-32). In adipocytes, fasting downregulates G0S2 expression, which in turn enhances ATGL-mediated intracellular lipolysis. Consistently, *G0s2*-deficient (*G0s2*$^{-/-}$) mice preferentially utilize FAs as an energy substrate, and their WAT exhibits enhanced lipolytic activity and increased thermogenic capacity (27, 30-32). In response to a high-fat diet (HFD), these mice remain lean, insulin sensitive, and resistant to weight gain and the development of hepatic steatosis (27, 30, 31).

In the present study, we focused on the metabolic impact of *G0s2* ablation in a mouse model of hypertriglyceridemia and atherosclerosis. Specifically, we investigated the role of G0S2 in the regulation of LPL and ANGPTL4 in adipose tissue. Our data provide compelling evidence that by acting as a switch for both ATGL-mediated intracellular lipolysis and LPL-mediated intravascular lipolysis, G0S2 in adipocytes is critically involved in regulating systemic TG clearance and the development of diet-induced dyslipidemia.

Results

G0S2 contributes to diet-induced hypertriglyceridemia but not hypercholesterolemia.

To evaluate the consequence of *G0s2* ablation on diet-induced hyperlipidemia and atherosclerosis, we treated *G0s2*$^{-/-}$ mice and their wild-type (WT) littermates with the atherogenic Western Diet (21.2% fat, 34% sucrose, and 0.2% cholesterol by weight) for 12 weeks. Concurrently, the mice were injected weekly with either a control antisense oligonucleotide (ASO) or an ASO specifically targeting LDL receptor (Ldlr-ASO) in the liver to create conditions of hypertriglyceridemia and hypercholesterolemia (33) (Figure 1A). At the end of the study, knockdown of hepatic *Ldlr* and knockout of *G0s2* expression were confirmed by Western blotting analysis (Figure 1B). In mice receiving the control ASO, no differences in the plasma levels of TG or cholesterol including total, free and esterified cholesterol were observed between the two genotypes (Figure 1C and 1D). Upon *Ldlr* knockdown, the plasma levels of TGs and cholesterol elevated by 2.6- and 3.6-fold, respectively, in the WT mice. Interestingly, the *G0s2*$^{-/-}$ mice receiving the Ldlr-ASO were fully protected against the development of hypertriglyceridemia but not hypercholesterolemia (Figure 1C and 1D). Specifically, the *G0s2*$^{-/-}$ mice exhibited normal fasting plasma TG levels (Figure 1C) as well as a drastic reduction in TG content of all lipoprotein fractions including VLDL, LDL and HDL (Figure 1E). In comparison, neither total plasma nor lipoprotein-associated cholesterol content was significantly affected by *G0s2* ablation (Figure 1D and 1F), though the size of LDL appeared to increase in the *G0s2*$^{-/-}$ mice receiving Ldlr-ASO (Figure 1F). Plasma free FA levels also remained similar between the two genotypes (Figure 1G). Furthermore, combinational treatment with Western diet and Ldlr-ASO promoted atherosclerotic development in both WT and *G0s2*$^{-/-}$ mice (Figure 2A-2D).

However, Oil Red O-staining of the aortic root cross-section demonstrated a more pronounced lipid deposition in the WT mice than the *G0s2*$^{-/-}$ mice (Figure 2B). En face Sudan IV staining of the entire aorta revealed plaques predominantly localized at the aortic root (Figure 2C). Quantitative analysis of the Sudan IV-positive area indicated that WT mice had a greater total burden of plaques compared to the *G0s2*$^{-/-}$ mice (Figure 2D). Taken together, these findings provide evidence that *G0s2* ablation confers resistance against diet-induced hypertriglyceridemia as well as reduces the severity of atherogenesis without affecting hypercholesterolemia.

_G0s2_ ablation decreases adiposity and increases whole-body lipid oxidation.

Along with alleviated hypertriglyceridemia, *G0s2*$^{-/-}$ mice showed less body weight gain and lower percentage of body fat mass than WT littermates when treated with Western diet and the Ldlr-ASO (Figure 3A and 3B). The difference in body weight gain between the two genotypes was abolished as the percentage of lean mass slightly increased in the *G0s2*$^{-/-}$ mice. Notably, no significant differences were observed in food consumption between WT and *G0s2*$^{-/-}$ mice (Figure 3C). A multi-day metabolic cage study showed a similar rate of oxygen consumption during both fasting and refeeding periods (Figure 3D). However, the respiratory exchange ratio (RER) was shifted significantly downward during fasting and refeeding in *G0s2*$^{-/-}$ mice (Figure 3E). In addition, *G0s2*$^{-/-}$ mice showed a significant increase in the total energy expenditure in the refeeding period (Figure 3F). These results suggest that *G0s2* ablation promotes overall energy consumption and the preference of lipids to carbohydrates as energy substrate, which is consistent with enhanced ATGL-mediated lipolysis.

_G0s2_ ablation improves whole-body TG clearance without impacting hepatic TG secretion.

To further establish the link between G0S2 and hypertriglyceridemia, we conducted an oral lipid tolerance test (OLTT) in *G0s2*$^{-/-}$ mice and their WT littermates. As described above, knockdown of hepatic Ldlr caused a more pronounced increase in the fasting plasma TG levels in WT than *G0s2*$^{-/-}$ mice on the Western diet. In the WT mice, an oral gavage of olive oil led to a sharp rise in plasma TG levels, which peaked at the 2-h timepoint and then slowly declined over the next 4 h (Figure 4A). However, in the *G0s2*$^{-/-}$ mice, the initial increase was significantly dampened after the 1-h timepoint, resulting in a significantly lower peak value at the 2-h time point (Figure 4A). Comparison of Incremental Area Under the Curve (AUC) showed a quantitative improvement of oral lipid tolerance in the *G0s2*$^{-/-}$ mice (Figure 4B).

Despite drastically decreased hepatic TG content (Figure 4C) and a loss of lipid vacuoles in the liver sections (Figure 4D), *G0s2*$^{-/-}$ mice showed no difference from the WT mice in the rate of hepatic TG secretion as measured after treatment with Poloxamer-407 (Figure 4E), a lipoprotein lipase inhibitor. Since intestinal lipid absorption as reflected by fecal TG content was also comparable between the two mouse lines (Figure 4F), we hypothesized that *G0s2* deficiency would lead to increased plasma TG clearance. To this end, we analyzed the TG lipase activity in the plasma. As shown in Figure 4G, *G0s2*$^{-/-}$ mice had significantly increased plasma lipase activity both before and after heparin injection. While it was increased by 33.78% prior to heparin injection, post-heparin plasma lipase activity in *G0s2*$^{-/-}$ mice was increased by 29.93% compared to the WT mice (Figure 4G). These data implicate elevated circulating LPL in the alleviation of diet-induced hypertriglyceridemia in the *G0s2*$^{-/-}$ mice lacking hepatic Ldlr.

***G0s2* ablation increases oral lipid tolerance and LPL production in chow-fed mice.**

Similar to what was observed under the hypertriglyceridemic condition, *G0s2*$^{-/-}$ mice fed a chow diet exhibited an improved oral lipid tolerance when compared to the WT mice (Figure 5A and 5B). While no differences in intestinal lipid absorption were observed between WT and *G0S2*$^{-/-}$ mice (Figure 5C), plasma lipase activities, both pre- and post-heparin, were elevated by more than sixfold in *G0s2*$^{-/-}$ mice (Figure 5D). Plasma concentrations of LPL protein showed a similar increase in the *G0s2*$^{-/-}$ mice (Figure 5E), suggesting a physiological role of G0S2 in intravascular lipolysis through the regulation of LPL production. Measurement of tissue specific post-heparin lipase activity showed an increase in the WAT and heart by 195% and 77%, respectively, upon *G0s2* ablation (Figure 5F). To identify the tissues responsible for the enhanced lipid clearance, we analyzed lipid uptake using a [^{3}H]-labeled triolein tracer. Figure 5G shows that *G0s2*$^{-/-}$ mice displayed increased lipid uptake mainly in the WAT as compared with the WT control. Furthermore, the tissue-specific role of G0S2 was demonstrated in adipose-specific *G0s2* knockout (*G0s2*-AKO), which exhibited improved oral lipid tolerance (Figure S1A and S1B), accompanied by elevated pre- and post-heparin circulating lipase activities and LPL protein levels (Figure S1C-S1D). Taken together, the results suggest that increased LPL production from WAT likely contributes to enhanced TG clearance in *G0s2*$^{-/-}$ mice.

Transplantation with *G0s2*$^{-/-}$ WAT alleviates diet-induced hypertriglyceridemia in WT recipient mice.

Increased LPL activity in the WAT prompted us to examine the WAT-specific effect of *G0s2* ablation. Specifically, we tested whether transplantation of WAT from *G0s2*$^{-/-}$ mice would improve diet-induced hypertriglyceridemia. To this end, we isolated epididymal fat pads from chow-fed WT or *G0s2*$^{-/-}$ mice and transplanted them into WT recipients (Figure 6A). Prior to the

experiment, donor mice showed no discernible differences in plasma TG levels (Figure S1A). The recipients were pre-fed with the Western diet for 3 weeks. At transplantation, the recipients had already developed hypertriglyceridemia, with plasma TG levels elevated by over two-fold compared with the chow-fed donors (Figure 6B and Figure S1A). After WT fat transplantation, the hypertriglyceridemia persisted, with plasma TG continuing to climb and reaching a plateau at the 2-week time point (Figure 6B). In comparison, transplantation with *G0s2*$^{-/-}$ fat completely reversed the hypertriglyceridemia, decreasing the plasma TG to levels even below those observed in the chow-fed donors (Figure 6B and Figure S1A). Consistent with the normalized TG levels, mice receiving the *G0s2*$^{-/-}$ fat graft exhibited significantly higher LPL activity and protein concentration in the plasma than those receiving the WT fat (Figures 6C and 6D). The effects appeared to be specific for plasma TG and LPL as there were no differences in the plasma levels of free FA, cholesterol or glucose between mice transplanted with WT and *G0S2*$^{-/-}$ fat (Figures 6E-6G). Body weight and body composition also remained unchanged between the two groups (Figure S1B and Figure S1C). Interestingly, transplantation with *G0S2*$^{-/-}$ fat led to a significant reduction in hepatic TG content (Figure 6H). Decreased plasma level of the ketone body β-hydroxybutyrate suggests decreased flux of FAs to liver for oxidation in mice receiving the *G0S2*$^{-/-}$ fat (Figure 6I). These results suggest that LPL produced from the *G0S2*$^{-/-}$ WAT is a major contributor to the circulating pool of the WT recipients, and transplantation of *G0s2*$^{-/-}$ WAT reverses diet-induced hypertriglyceridemia and improves hepatic steatosis.

***G0s2* ablation causes opposite changes in LPL and ANGPTL4 expression in WAT.**

LPL in WAT is downregulated during fasting and upregulated primarily by insulin during refeeding (34, 35). In comparison to wild-type (WT) mice, the *G0s2*$^{-/-}$ mice displayed a 59%

increase in fasting plasma LPL activity, which was further elevated by 66% upon insulin injection (Figure 7A). Relative to that in the WT mice, adipose LPL activity in the *G0s2*$^{-/-}$ mice was increased by 143% and 48%, respectively, under fasted and insulin-stimulated conditions (Figure 7B). Interestingly, the increases in adipose LPL activity were mirrored by elevations in the expression of LPL protein but not its mRNA. During refeeding, we observed a significant increase in the expression of LPL protein in the WAT of both *G0s2*$^{-/-}$ and *G0s2*-AKO mice (Figure 7C and Figure S1E), while *Lpl* mRNA levels remained unchanged (Figure 7D and Figure S1F). To determine the mechanisms by which LPL protein is regulated in *G0s2*$^{-/-}$ WAT, we analyzed the expression of three ANGPTL family members that are known to post-translationally downregulate LPL. To this end, we observed a significant downregulation of both ANGPTL4 protein and *Angptl4* mRNA in the *G0s2*$^{-/-}$ WAT compared to that in the WT WAT (Figure 7C and 7D; Figure S1E and S1F). On the other hand, *G0s2* ablation did not appear to affect the expression of *Angptl8* (Figure 7D; Figure S1F). By activating Akt-mediated phosphorylation, insulin is known to suppress FoxO1 activity, which can lead to decreased *Angptl4* transcription(36, 37). Consistent with decreased *Angptl4* expression, we observed increased activating phosphorylation of Akt (Ser473) as well as inactivating phosphorylation of FoxO1(Thr24) in WAT during refeeding (Figure 7C).

To directly test the effects of G0S2 loss on LPL and ANGPTL4, we transfected differentiated 3T3-F442A adipocytes with either a control siRNA or an established siRNA targeting *G0s2* (G0S2-siRNA). As shown in Figure 7E and 7F, both *G0s2* mRNA and G0S2 protein expression were efficiently knocked down in cells receiving the G0S2-siRNA. In the absence of G0S2, cells exhibited increased expression of LPL and decreased expression of ANGPTL4. While changes

in ANGPTL4 occurred at both protein and mRNA levels, G0S2 knockdown only affected the expression of LPL protein but not its mRNA (Figure 7E and 7F). In G0S2-knockdown cells, co-knockdown of ANGPTL4 did not further increase LPL protein abundance (Figure 7E), indicating a causal relationship between decreased ANGPTL4 expression and increased LPL abundance in adipocytes lacking G0S2. Furthermore, under the condition of serum deprivation, G0S2 knockdown resulted in increased response to insulin as shown by Western blotting analysis of phospho-Akt and phospho-FoxO1 (Figure 7G). Together, these data demonstrate that *G0s2* ablation leads to increased LPL protein expression in adipocytes, which is accompanied by enhanced insulin signaling and decreased expression of ANGPTL4.

Absence of G0S2 increases LPL protein stability in adipocytes.

As ANGPTL4 is known to promote intracellular degradation of LPL protein (20, 21), we then measured the protein stability of LPL in 3T3-F442A adipocytes where G0S2 was knocked down. To this end, we treated cells with cycloheximide (CHX), a protein synthesis inhibitor, to determine LPL protein half-life and whether LPL degradation rate is affected by G0S2. Upon CHX treatment, G0S2 knockdown slowed down the decay of LPL protein, increasing its half-life from ~15 min to ~30 min at basal state (Figure 8A and 8D) and from ~13 min to ~32 min in insulin-stimulated condition (Figure 8B and 8E). Interestingly, treatment of cells with Atglistatin, a specific chemical inhibitor of ATGL, was able to reverse the degradation rate of LPL in G0S2-knockdown cells to that in the control cells (Figure 8C and 8F). Similarly, adipocytes derived from the stromal vascular fraction (SVF) of *G0s2*$^{-/-}$ WAT showed increased expression of LPL protein along with decreased expression of ANGPTL4 (Figure 8G). CHX-chase experiments demonstrated enhanced protein stability of LPL in the *G0s2*$^{-/-}$ cells based on quantitative analysis

of protein bands after loading normalization (Figure 8H). Thus, G0S2 inhibition of ATGL-mediated lipolysis plays a significant role in the control of LPL protein stability, possibly through upregulation of ANGPTL4 expression.

Discussion

LPL and ATGL are both highly expressed in adipose tissue. While LPL governs TG turnover intravascularly, ATGL does so intracellularly. Previous studies have identified them as key enzymes in regulating the balance between lipid storage and utilization (3-6). However, the coordinated regulation of LPL and ATGL has remained less defined. In the present study, we uncovered a common mechanism governing their control within adipose tissue. Our findings suggest that G0S2, a known inhibitor of ATGL, acts as a molecular off-switch for functional LPL protein production, thereby influencing intravascular lipolysis in adipose tissue and whole-body TG clearance. Furthermore, we provide evidence that this role is linked to the development of hypertriglyceridemia under specific dietary conditions.

Our study highlights the selective role of G0S2 in regulating systemic TG metabolism and its impact on atherosclerosis. The absence of G0S2 confers resistance to Western diet-induced hypertriglyceridemia in a mouse model with inducible hepatic *Ldlr* knockdown, as evidenced by significantly reduced fasting plasma TG levels across all lipoprotein fractions. Moreover, both global *G0s2*$^{-/-}$ and adipose-specific *G0s2*-AKO mice exhibit improved oral lipid tolerance and elevated circulating LPL levels, indicating enhanced TG clearance. Despite the protective effects against hypertriglyceridemia, *G0s2*$^{-/-}$ mice still develop atherosclerosis under atherogenic conditions. However, the extent of atherosclerotic progression is significantly reduced compared to WT mice, suggesting that *G0s2* ablation partially mitigates disease severity. This underscores the modulatory role of G0S2 in atherogenesis, where its absence reduces, but does not entirely prevent lesion development. A key innovation in our model is the use of a GalNAc-conjugated ASO that selectively targets hepatic *Ldlr* expression while sparing *Ldlr* in other cell types. This

selective approach preserves macrophage LDL receptor function, which may influence atherogenesis. Additionally, the lower TG/HDL ratio observed in *G0s2*$^{-/-}$ mice suggests a shift toward larger, less dense LDL particles. We hypothesize that these larger LDL particles are less readily taken up by macrophages, potentially reducing foam cell formation and slowing the progression of atherosclerosis.

Although G0S2 ablation has no impact on hepatic TG secretion, it enhances the whole-body respiratory exchange ratio (RER), implying that increased lipid oxidation combined with enhanced TG clearance contributes to mitigating hypertriglyceridemia in these mice. Additionally, the reduction in body weight gain and adiposity observed in *G0s2*-deficient mice align with increased lipolysis and oxidative lipid utilization. These findings further underscore the role of G0S2 in the regulation of whole-body lipid metabolism and energy homeostasis. That transplantation of *G0s2*$^{-/-}$ WAT completely normalized the circulating TG levels in the WT recipients with preexisting hypertriglyceridemia strongly indicates an adipose tissue-autonomous effect of *G0s2* ablation. The elevated circulating levels of LPL in the recipient mice indicate that LPL produced by the *G0s2*$^{-/-}$ WAT graft is a major contributor to the circulating pool, which presumably accelerates TG catabolism and lipid clearance. This in turn would lead to decreased circulating TG levels and diminished ectopic lipid accumulation in other peripheral tissues. In fact, a significant reduction in hepatic steatosis was observed in mice receiving the *G0s2*$^{-/-}$ WAT. Given the significant decline in plasma TG without any changes in body weight or fat mass, we speculate that TGs might be cleared through adipose tissue, where FAs derived from LPL action are either efficiently oxidized or stored as TGs that might be further hydrolyzed by ATGL and oxidized, or a combination of both. Indeed, prior research has demonstrated heightened lipolysis,

increased FA oxidation, and upregulated expression of brown-like genes in the WAT of *G0s2*$^{-/-}$ mice (27, 30, 31). One study has reported G0S2's regulatory role in thermogenesis and an augmentation in the expression of FA oxidation genes in the brown adipose tissue (BAT) of *G0s2*$^{-/-}$ mice (30). These findings align well with a study involving adipose tissue-specific ATGL-transgenic mice (38). Conversely, in mice with adipose tissue-specific ATGL deficiency, fat mass is preserved due to a decrease in *de novo* FA synthesis that compensates the decreased intracellular lipolysis in adipose tissue (39, 40).

An intriguing observation made during the present study is the role of G0S2 in modulating LPL production in WAT. The loss of G0S2 induces heightened intracellular lipolysis facilitated by ATGL. Both *G0s2*$^{-/-}$ and *G0s2*-AKO mouse models corroborates an earlier observation where the pharmacological inhibition of ATGL resulted in delayed clearance of post-prandial plasma TGs (41). While Atglistatin treatment significantly reduces *Lpl* mRNA expression in WAT, G0S2 seems to exclusively influence LPL protein expression without affecting its transcription in adipocytes. Mechanistically, the study elucidates that G0S2 inhibition of ATGL-mediated lipolysis plays a crucial role in controlling LPL protein stability in adipocytes. In this context, ANGPTL4 is known to inhibit LPL activity through various mechanisms, one of which involves reducing the intracellular stability of LPL protein (20, 21). This occurs by interacting with LPL and inducing its unfolding, thereby increasing susceptibility of LPL to proteolytic degradation. Consequently, the levels of functional LPL decrease. Thus, it is conceivable that by regulating ANGPTL4 expression and subsequent LPL degradation, G0S2 fine-tunes LPL production and secretion, thereby influencing systemic lipid homeostasis. The fact that co-knockdown of ANGPTL4 did not further increase LPL expression in *G0s2*-knockdown adipocytes supports

such a causative relationship. Interestingly, knockout of *Angptl4* in adipose tissue yielded similar metabolic phenotypes to *G0s2* ablation, including enhanced LPL activity, rapid clearance of circulating TGs, and increased FA oxidation, thereby preventing excessive ectopic lipid deposition in the liver and reducing hypertriglyceridemia (15, 17, 22).

What is the physiological benefit of G0S2-mediated downregulation of LPL in WAT during feeding? We propose that this regulation ensures that LPL-mediated uptake of TRL-derived FAs aligns with TG synthesis in white adipocytes, particularly under conditions where WAT is predominantly non-oxidative and for TG storage. By limiting FA uptake through controlled LPL activity, G0S2 may play a role in maintaining WAT homeostasis during feeding. In the absence of G0S2, however, WAT undergoes significant remodeling toward a more insulin-sensitive and oxidative state (27, 30, 31). In this remodeled state, increased LPL production likely facilitates greater FA uptake by adipocytes to support oxidative metabolism. This regulatory shift is accompanied by reduced *Angptl4* expression, which we observed to be linked with enhanced insulin signaling. Specifically, increased phosphorylation of Akt and FoxO1 in adipocytes following refeeding or insulin stimulation indicates heightened insulin responsiveness. Given the established role of FoxO1 in driving *Angptl4* expression (36, 37), we hypothesize that its increased phosphorylation and subsequent inactivation directly contribute to the observed reduction in ANGPTL4 levels. Furthermore, our findings are consistent with studies in adipose-specific ATGL transgenic mice (38), in which enhanced lipolytic activity in both BAT and WAT promotes mitochondrial FA oxidation, uncoupled respiration, and thermogenic energy dissipation. This metabolic shift alleviates insulin resistance, even under HFD conditions.

Collectively, these results highlight the critical role of G0S2 in modulating lipid metabolism, enhancing insulin sensitivity, and promoting metabolic flexibility in WAT.

In summary, the present study offers additional insights into the multifaceted role of G0S2 in lipid and energy metabolism. Understanding the intricate interplay among LPL, ANGPTL4, and G0S2 illuminates the complex regulation of adipose and whole-body TG metabolism. Targeting these regulatory pathways shows promise for developing new therapeutic strategies to manage hypertriglyceridemia and prevent its associated complications. Significantly, our findings that the transplantation of *G0s2*$^{-/-}$ WAT alleviates diet-induced hypertriglyceridemia further underscores the therapeutic potential of targeting G0S2 in lipid metabolism disorders.

Materials and Methods

Sex as a biological variable

We mainly examined male animals as the effects of Ldlr-ASO on plasma TG and cholesterol levels as well as atherogenesis are more prominent in male mice(42).

Animal

Global *G0s2* knockout mice on C57BL/6 background were produced as described previously(27). Heterozygous *G0s2*$^{+/-}$ mice were crossed to generate the homozygous *G0s2*$^{-/-}$ mice. 7-week-old male WT and *G0s2*$^{-/-}$ littermates were used for experiments. *G0s2*-AKO mice on C57BL/6 background were generated by crossing homozygous *G0s2* loxP-flanked (*G0s2*$^{fl/fl}$) mice (GemPharmatech Co., Ltd, Strain #: T013269) with Adipoq-Cre transgenic mice (Jackson Laboratory, Strain #:028020). The resulting heterozygous *G0s2*$^{fl/+}$ and hemizygous Adipoq-Cre mice were further crossed with homozygous *G0s2*$^{fl/fl}$ mice to generate homozygous *G0s2*-AKO mice. The homozygous *G0s2*$^{fl/fl}$ littermates were used as WT controls. All mice were housed in the animal facility at Mayo Clinic in Rochester with a 12-h light/dark cycle, a controlled humidity (40-70%), and a stable temperature (22 ±3°C), and given free access to water and diet except when fasting blood specimens were obtained. Mice were fed either a standard chow diet (Lab Diet, No. 5053) or Western diet (Research Diet, No. D12079B, 0.21% cholesterol), as indicated. Mice and diets were weighed weekly. Mice were subjected to EchoMRI scanning for body composition analysis. For atherosclerosis model building, 7-week-old WT and *G0s2*$^{-/-}$ mice were switched to Western diet and injected intraperitoneally with either a control ASO or a

GalNAc-conjugated Gen 2.5 *Ldlr* ASO (kind gift from Ionis Pharmaceuticals, Carlsbad, CA) at a dose of 5mg/kg body weight once a week for 12 weeks.

Protein extraction and Western blot analysis

Total proteins were extracted from cells or tissues using 1X RIPA buffer (150mM NaCl, 1% Triton X-100, 0.1% SDS, 0.5% Sodium deoxycholate, 1mM EDTA and 50nM Tris pH 7.4) with cOmplete™ EDTA-free Protease Inhibitor (Sigma-Aldrich, No.11836170001). Protein concentration was determined using a Pierce BCA protein assay kit (Thermo Scientific, No.23225). Total protein was loaded and separated by SDS-polyacrylamide gel electrophoresis (SDS-PAGE) and transferred to a 0.2 μm nitrocellulose membrane (Bio-Rad, No.1620112). After blocking membranes in 5% milk in TBST (150mM NaCl, 15.2mM HCl, 4.62mM Tris-Base, 0.1% Tween 20) for 5 minutes at room temperature, primary antibodies diluted in 5% milk were added to the membranes and incubated on shaker at 4°C overnight. The following rabbit polyclonal or mouse monoclonal primary antibodies were used: anti-mouse LDLR (R&D Systems, No. AF2255), anti-mouse G0S2 (affinity-purified rabbit polyclonal custom generated by Proteintech Group, Inc) (26), anti-human/mouse LPL (R&D Systems, No. AF7197), anti-human/mouse ANGPTL4 (Proteintech, No.67577), anti-mouse FoxO1 (Cell signaling, No. 2880), anti-mouse phospho-FoxO1 (Cell signaling, No.2599), anti-mouse Akt (Cell signaling, No.9272), anti-mouse phospho-Akt(Ser473) (Cell signaling, No.9271), anti-β-actin (Santa Cruz Biotechnologies, sc-8432). After overnight incubation, membranes were incubated at room temperature for 1 h with the corresponding goat anti-mouse (Thermo Fisher Scientific, No. PA186015), goat anti-rabbit (Thermo Fisher Scientific, No. 65-612-0) or donkey anti-goat (Jackson ImmunoResearch, No. 705-035-147) horseradish peroxidase (HRP)-conjugated

secondary antibodies diluted in 5%milk in TBST. Proteins were visualized by SuperSignal West Pico PLUS Chemiluminescent Substrate (Thermo Fisher Scientific, 34580) and imaged using ImageQuant LAS4000 instrument (GE Healthcare). Western blot data were collected from a minimum of three independent experiments, and a representative membrane is depicted in the figures.

Blood sampling

All blood samples were collected after either overnight or 4 h of fasting. For OLTT and hepatic TG secretion assay, small amounts of blood were collected from submandibular vein. Mice were restrained by grasping over the shoulders. A 25-gauge lancet was used to puncture the vessel at a shallow depth of 1-2 mm. Serial sampling was done using alternate sides of the face. Otherwise, blood samples were collected from retro-orbital plexus of mice using microhematocrit capillary tubes (Fisher Scientific, No.22-362574) and save in EDTA-coated collectors (RAM Scientific, No. 076011). Blood was centrifuged at 12,000g for 15min for cell precipitation and collection of the plasma. For LPL activity and concentration measurement, freshly collected plasma was used. In other cases, plasma was aliquoted and frozen at -80℃ for further experiments.

Plasma lipid measurement

Plasma TG was determined by Infinity Triglyceride Reagent (Thermo Scientific, No. TR22421), according to the manufacturer's instructions. An aliquot of each sample was mixed with reagent at 1:100, incubated at 37℃ for 5 min and then read by a microplate reader. Plasma cholesterol levels were measured using the Amplex™ Red Cholesterol Assay Kit (Thermo Scientific, No. A12216), according to the manufacturer's instructions. Each sample was mixed at 1:1 dilution

with Reaction Buffer containing 300μM Amplex™ Red reagent, 2U/mL HRP, 2U/mL cholesterol oxidase, with or without 0.2U/mL cholesterol esterase for either total cholesterol or cholesterol ester measurements. After incubation at 37℃ for at least 30 min, protected from light, the fluorescence was read using excitation between 530-560 nm and emission at ~590nm. Free cholesterol could be obtained by subtraction of cholesterol ester from total cholesterol. Plasma free FA was assessed by Wako HR Series non-esterified FA assay kit (FUJIFILM Wako Chemicals, No. 997-76491), according to the manufacturer's instructions. Briefly, each plasma sample was diluted in Color Reagent A at 1:20 and incubated at 37℃ for 10 min, followed by mixing with Color Reagent B at 2-fold of Reagent A and another 10-min incubation at 37℃. Absorbance at 550nm of the samples at room temperature was obtained by microplate reader and used to calculate non-esterified FA concentrations. Three replica measurements were performed for each sample group and reported as mg/dL for TG and cholesterols, and mmol/L for non-esterified FA.

Fast-protein liquid chromatography

Fast-protein liquid chromatography (FPLC) analysis was performed at the Analytic Services Core of Vanderbilt Diabetes Research and Training Center. Specifically, 100 μl of plasma pooled from 6 mice per group was separated on a Superose 6 column (Amersham Pharmacia). Forty 0.5-ml fractions were collected. Cholesterol and TG analyses were performed on each fraction using standard enzymatic assays. Fractions 16–24 contain VLDL; 25–44, LDL and 45–53, HDL. HDL cholesterol was measured with the enzymatic method after precipitation of VLDL and LDL using polyethylene glycol reagent (PEG). From these data LDL cholesterol was calculated using the Friedewald equation.

Atherosclerotic lesion analysis

Each anesthetized mouse was perfused with PBS. The aorta was then exposed, and fat was carefully removed. Pictures of the aortic root and branches were taken using a digital camera. Sever innominate, carotid, and subclavian arteries of aortic arch in thoracic aorta, and iliac arteries in abdominal aorta 3-5 mm after the bifurcations. The root of heart and whole aortas were collected in 10% formalin, kept overnight at 4°C, and then stored in 70% ethanol at 4°C for further processing. For cross section analysis, the root of the heart and ascending aorta was cut and embedded in Tissue-Tek optimal cutting temperature compound (O.C.T, SAKURA, No.4583), frozen, and stored at −20°C. Serial longitudinal cryostat sections (4μm) were made using Leica cryostat, mounted on SuperFrost Plus Slides (Cardinal Health, No. m6146-plus) and stained with Oil-red O. Slides were scanned by MoticEasyScan Pro 6-FS (Motic). *En face* analysis of lesions was performed as previously reported. Briefly, the entire aorta was dissected from the proximal ascending aorta to the bifurcation of the iliac artery along the outer curvature until the aortic arch resembles a Y-shaped split. Then the Y-shaped aortas were flattened and pinned onto a black wax petri dish, fixed with 4% buffered paraformaldehyde overnight. On next day, the aortas were washed with 70% ethanol solution twice, followed by staining with Sudan IV staining solution (1% Sudan IV in acetone, diluted with equal volume of 70% ethanol) at room temperature for 10 min. Afterwards, aortas were briefly washed with 80% ethanol solution for three times. Images of the stained aortas were taken with PBS filling the black wax petri dish and analyzed with ImageJ software to quantify lesion areas. Quantification data were shown as percentage of Sudan IV positive area normalized to the whole aorta.

Metabolic cage analysis

All experimental mice were individually housed in the comprehensive laboratory animal monitoring system equipped with photocells (CLAMS equipped with an Oxymax Open Circuit Calorimeter System; Columbus Instruments) and fed either standard chow diet or WD. After a 16 h acclimation period, metabolic data were continuously collected over a 72-h period that included 24 h of *ad libitum* feeding with indicated diet followed by 24 h of fasting and 24 h of refeeding. The VO_2 and VCO_2 values will be used to calculate the RER, and VO_2 and RER values will be used to determine the basal metabolic rate (kcal/kg/h). Data were normalized with lean body weight per hour and compared between groups by mean of each light or dark cycle.

Orla lipid tolerance test (OLTT)

OLTT was performed as previously described(43). Briefly, all experimental mice were oral gavage administered with olive oil (100µl/20g body weight) followed by a 4-h fasting period for clearance of dietary chylomicrons. Submandibular sampling was used to collect plasma right before as well as at 2-, 4- and 6-h time point post olive oil administration. The area under the 6-h plasma TG curve (AUC) were calculated by the trapezium rule. To adjust for the variations in baseline levels, the incremental AUC (iAUC) was calculated with baseline values subtracted as described previously (44).

Liver lipid measurement

Liver extracts were obtained by homogenizing 100-300 mg of liver in 350 µL of ethanolic KOH. Homogenates were then incubated overnight at 55° C. Digested tissue was diluted in H_2O: Ethanol (1:1) to a final volume of 1 mL. Samples were microcentrifuged for 5 minutes, and supernatant transferred to a new tube. Volume of supernatant was totaled at 1.2 mL with H_2O:

Ethanol (1:1). A volume of 200 µL was transferred to a new tube where 215 µL of 1 M $MgCl_2$ was added. Samples were then vortexed, incubated on ice for 10 minutes and microcentrifuged for 5 minutes. Supernatant was transferred to a new tube and used for liver lipid assessment according to the manufacturer's protocol. Liver TG and cholesterol were assessed in each animal of all groups and reported as mg/g liver.

Histology

Liver tissue was fixed in 10% formalin, embedded in paraffin (FFPE), and sectioned at 10 µm in the Mayo Clinic Pathology Core. Sections were stained with hematoxylin and eosin (H&E). Stained slides were imaged by MoticEasyScan Pro 6-FS (Motic).

***In vivo* hepatic TG secretion assay**

Hepatic TG secretion was determined by blocking VLDL catabolism using Poloxamer-407 (1g/kg body weight in PBS, i.p. injection) after a 4-h fast. Plasma was collected immediately before, and at 1-, 2-, 6- and 18-h timepoint after administration of Poloxamer-407. Plasma TG levels were measured as described above.

Fecal TG measurement

Fecal lipids were collected and extracted from mouse feces as described previously (45). Experimental mice were individually housed with small particle bedding. Mice were fed *ad libitum* with either chow diet or Western diet as indicated for 7 days. At the end of study, mice were placed in new cages and bedding in the old cages was collected for lipid extraction. Feces in old bedding were collected, weighed and ground into powder. 1 g of powdered feces per

mouse was used for lipid extraction following the same method applied for liver TG extraction. Fecal TG content was shown as mg/g of feces.

Lipase activity and LPL concentration analysis

Mouse plasma was collected 10 min after intraperitoneal injection with PBS or heparin (100U/kg in PBS). In some experiments, epididymal WAT (eWAT) were freshly dissected out of WT and G0S2$^{-/-}$ mice. The adipose was weighed and cut into small pieces and immediately put into phenol red-free DMEM culture media for 30 min with or without heparin (50IU/mL). Media was collected for LPL activity measurement. LPL activity was assessed by LPL Activity Assay Kit (Sigma-Aldrich, No.MAK109), according to manufacturer's instructions. 5 μL of each sample (either plasma or cultured media) was mixed with 194 μL of LPL Assay Buffer and 1μL of LPL substrate emulsion in a microplate. The plate was sealed and incubated at 37℃ for 15 min to 60 min. The fluorescence read upon excitation at 370nm and emission at 450nm from each sample was used for determination of LPL activity. LPL activity was measured in triplicate and reported as μM/min for plasma or μM/g·min for eWAT explants.

Plasma LPL concentration was determined by LPL ELISA kit (MyBioSource, No. MBS701545). Fresh plasma was collected from WT and G0S2$^{-/-}$ mice 10min after PBS or heparin administration. 100 μL plasma was added into each well and incubated at 37℃ for 2 h. 100μL biotin-antibody was added into each well after removal of sample and incubated for 1hr at 37℃. Plate was washed with Wash Solution three times and liquid was completely removed. After adding 100 μL of HRP-avidin to each well, the plate was incubated at 37℃ for another 1h. 90 μL of TMB Substrate was added after another five washes. Plate was subjected to a 30min

incubation at 37°C. Stop Solution was then added by 50μL/each well and plate was rea at 450nm for determination of LPL concentrations. Results were reported as ng/mL.

Tissue isotope tracing assay

Before the experiment period, WT and G0S2$^{-/-}$ mice were fed *ad libitum* from 6pm to 6am and fasted from 6am to 6pm for 5 days to achieve metabolic synchronization. On the day of experiment, mice were fasted for 4h to ensure chylomicron clearance and then given 200μL of olive oil containing ^{3}H-triolein(1μCi) via oral gavage. Liver, heart, epididymal WAT, BAT and skeletal muscle (quadriceps) were harvested 4h after oral gavage, and the specific radioactivity of ^{3}H was measured using a liquid scintillation counter. DPM readings were normalized to tissue mass.

Adipose tissue transplantation

Procedures were performed under isoflurane-induced anesthesia as described previously (46, 47). Briefly, epididymal fat pads were dissected from age-matched chow-fed WT and G0S2$^{-/-}$ male mice and transplanted *in situ* into WT mice pretreated with the Western diet (n=9 WT recipients, n=10 G0S2$^{-/-}$ recipients). Before transplantation, small incisions were made in the lower abdominal region of anesthetized donor and recipient mice to expose the epididymal fat pads. Donor fat pads were dissected, placed in sterile saline, and cut into 100-mg pieces. These grafts were implanted into the recipient's epididymal fat pads and secured by sutures. Each recipient received 100 mg of donor fat per side (200 mg total). Skin incisions were closed using 5-0 silk sutures. After transplantation the recipient mice were monitored weekly for plasma TG levels.

Four weeks post-transplantation and after overnight fasting, tissues and plasma were collected following euthanasia.

Plasma glucose and β-hydroxybutyrate measurement

After an overnight fast, blood samples were then obtained from the tail vein, and the blood glucose level was measured using a Contour glucometer (Bayer). Fasting plasma β-Hydroxybutyrate was determined by β-Hydroxybutyrate (Ketone Body) Colorimetric Assay Kit (Cayman Chemical, No. 700190), according to manufacturer's instructions. Briefly, each plasma sample was mixed with equal volume of Developer Solution in each well and incubate at 25℃ in the dark for 30min. Absorbance at 450 could be used for BHB calculation.

Cell culture, treatment, and siRNA transfection

3T3-F442A preadipocytes (Sigma-Aldrich, CB_ 00070654) were maintained and differentiated as previously described (48). Cells were maintained in DMEM (Gibco, No.11995-065) supplemented with 10% newborn calf serum (ATCC, No.30-2030) and 1% Penicillin/Streptomycin (Thermo Scientific, No.15140122) in a humidified atmosphere containing 10% CO_2 at 37℃. Two days after confluence (Day0), cells were replaced in differentiation media I (DMEM containing 10% fetal bovine serum (FBS, Thermo Fisher Scientific, No.10-437-028), 1%P/S, 1μg/ml insulin (Sigma, No. I5523), 0.25μM dexamethasone (Sigma, No. D-4902) and 0.5 mM methyl isobutylxanthine (IBMX, Sigma, No. I-7018) for 3 days. Then the media was removed and changed to Differentiation Media II (DMEM containing 10% FBS and 1μg/ml insulin). Two days after in insulin-containing medium, the cells were then cultured in DMEM containing 10%FBS for another 2 days. On Day 7-8, full differentiated cells

are trypsinized and resuspend in PBS and subjected for siRNA knockdown via electroporation as described previously (49). Briefly, either 5 μM of an established G0S2-specific siRNA(27) or a GC-matched control siRNA was mix with 500μL of adipocyte suspension in PBS in 4-mm electroporation cuvette and pulsed at 950μF and 160V by Bio-Rad Gene Pulser Xcell electroporator. Three days after electroporation, cells were either harvested for protein separation/mRNA extraction or treated with cycloheximide (50μg/mL), insulin (100nM), and Atglistatin (10μM) for appropriate timepoints.

Isolation and adipogenic differentiation of mouse SVF cells

Epididymal fat pads were minced into small pieces and placed in digestion buffer (DMEM supplemented with 1% P/S, 20 mg/mL bovine serum albumin (BSA Sigma-Aldrich, No. A6003), 10 mM $CaCl_2$ and 2mg/mL collagenase (Sigma-Aldrich, No. C5138) at 37℃ with constant agitation at 150 rpm for ~30min. Complete DMEM containing 10% FBS and 1% P/S was then added to stop digestion. The mixture was centrifuged at 700g for 10 min. The fat layer was discarded, and SVF as the pellet was resuspended in 10% FBS containing DMEM and filtered over a 40μM strainer. Another centrifugation was then applied to remove death cells and debris. SVF was finally plated on collagen I (Thermo Scientific, No. A1048301)-coated plates in complete DMEM. SVF differentiation was induced by replacement confluent cells with Adipogenic Medium 2 (High glucose DMEM containing 10%FBS, 1% P/S, 8mg/L biotin, 4mg/L pantothenate, 10mg/L transferrin,1mg/L insulin, 0.1μM hydrocortisone, 0.2μM Triiodo-L-thyronine (T3), 0.25μM dexamethasone, 0.5μM IBMX, and 2μM Rosiglitazone). 4 days later, the medium was then removed, and cells were incubated with DMEM supplemented with

10%FBS, 1% P/S, 8mg/L biotin, 4mg/L pantothenate, 10mg/L transferrin,1mg/L insulin, 0.1μM hydrocortisone, 0.2μM Triiodo-L-thyronine (T3) for another 4-6 days.

RNA extraction and quantitative real-time PCR (qPCR) analysis

Total RNA was extracted from cells and tissue using PureLink RNA Mini Kit (Thermo Fisher Scientific, No.12183025) and Ambion TRIZol Reagent (Thermo Fisher Scientific, No.15-596-018), according to manufacturer's instructions, respectively. Complementary DNA (cDNA) was synthesized from 0.4 μg of total RNA using High-Capacity cDNA Reverse Transcription Kit (ThermoFisher, No. 4368813). Quantitative real-time PCR was performed using Itaq Universal SYBR green master mix (Bio-Rad, No.1725124) on a CFX96 Touch Real-time PCR machine (Bio-Rad) or QuantStudio VII instrument (Life Technologies). Each sample was tested in duplicate or triplicate. To determine the fold-change in gene expression compared to a control group, ΔΔCt was calculated. To determine the relative expression of corresponding genes, ΔCt was determined.

Quantification and statistical analysis

All graphs and statistical analyses were generated using GraphPad Prism 10. Bar graphs represent Mean + S.E.M. *P* values were determined by two-tailed student's t-test or ANOVA using GraphPad Prism 10. Statistical details can be found within the figures, with legends for *P* values indicated in figure legends. Where deemed necessary, ns was included to emphasize no statistical significance; where no value is given, no significance was present.

Study approval

The Institutional Animal Care and Use Committee (IACUC) at Mayo Clinic approved all animal studies in accordance with federal guidelines. The Mayo Clinic IACUC protocol A00005548-20-R23 covering the included studies was initially approved on October 7, 2020, and reapproved on September 21, 2023 (expires September 21, 2026).

Data availability

All data are available in the main text or the supplementary materials. Source Data values are provided with this paper. Any additional information required to reanalyze the data reported in this paper is available from the lead contact upon request.

Author Contributions Statement

Y.C. designed and performed research, analyzed data, and wrote the manuscript. S.M.J., S.D.B., D.P., A.M.A. and C.E.M. performed research, analyzed data and edited the manuscript. J.L. designed and supervised the study as well as wrote and edited the manuscript. J.L. is the guarantor of this work and, as such, had full access to all the data acquired in the study, and takes responsibility for the integrity of the data and the accuracy of the data analysis.

Acknowledgements

We would like to thank Dr. Bennett Childs for sharing technical expertise in atherosclerotic analysis, Dr. Thomas White for assisting in mouse metabolic cage study, and Drs. Jielu Hao and Jinghua Hu for advising on mouse fat transplantation procedure. This publication was supported by research grants to J.L. from the National Institute of Diabetes and Digestive and Kidney Diseases (DK109096 and DK130331), post-doctoral T32 grant to S.D.B. from the National Institute of Diabetes and Digestive and Kidney Diseases (DK007352), as well as pre-doctoral funding to S.M.J. from the Mayo Foundation for Medical Education & Research and predoctoral T32 program from the National Institute of Diabetes and Digestive and Kidney (DK124190). The Lipid Core Laboratory of the Mouse Metabolic Phenotyping Center (MMPC) at Vanderbilt University is supported by DRTC grant from the National Institute of Diabetes and Digestive and Kidney Diseases (DK020593).

References

1. Zwick RK, Guerrero-Juarez CF, Horsley V, and Plikus MV. Anatomical, Physiological, and Functional Diversity of Adipose Tissue. *Cell Metab.* 2018;27(1):68-83.
2. Fruhbeck G. Overview of adipose tissue and its role in obesity and metabolic disorders. *Methods Mol Biol.* 2008;456:1-22.
3. Zhang R, and Zhang K. A unified model for regulating lipoprotein lipase activity. *Trends Endocrinol Metab.* 2024.
4. Wu SA, Kersten S, and Qi L. Lipoprotein Lipase and Its Regulators: An Unfolding Story. *Trends Endocrinol Metab.* 2021;32(1):48-61.
5. Yang A, and Mottillo EP. Adipocyte lipolysis: from molecular mechanisms of regulation to disease and therapeutics. *Biochem J.* 2020;477(5):985-1008.
6. Grabner GF, Xie H, Schweiger M, and Zechner R. Lipolysis: cellular mechanisms for lipid mobilization from fat stores. *Nat Metab.* 2021;3(11):1445-65.
7. Young SG, Fong LG, Beigneux AP, Allan CM, He C, Jiang H, et al. GPIHBP1 and Lipoprotein Lipase, Partners in Plasma Triglyceride Metabolism. *Cell Metab.* 2019;30(1):51-65.
8. Alves M, Laranjeira F, and Correia-da-Silva G. Understanding Hypertriglyceridemia: Integrating Genetic Insights. *Genes (Basel).* 2024;15(2).
9. Zhang X, Qi R, Xian X, Yang F, Blackstein M, Deng X, et al. Spontaneous atherosclerosis in aged lipoprotein lipase-deficient mice with severe hypertriglyceridemia on a normal chow diet. *Circ Res.* 2008;102(2):250-6.
10. Beigneux AP, Davies BS, Gin P, Weinstein MM, Farber E, Qiao X, et al. Glycosylphosphatidylinositol-anchored high-density lipoprotein-binding protein 1 plays a critical role in the lipolytic processing of chylomicrons. *Cell Metab.* 2007;5(4):279-91.
11. Kumari A, Kristensen KK, Ploug M, and Winther AL. The Importance of Lipoprotein Lipase Regulation in Atherosclerosis. *Biomedicines.* 2021;9(7).
12. Takahashi M, Yagyu H, Tazoe F, Nagashima S, Ohshiro T, Okada K, et al. Macrophage lipoprotein lipase modulates the development of atherosclerosis but not adiposity. *J Lipid Res.* 2013;54(4):1124-34.
13. Babaev VR, Fazio S, Gleaves LA, Carter KJ, Semenkovich CF, and Linton MF. Macrophage lipoprotein lipase promotes foam cell formation and atherosclerosis in vivo. *J Clin Invest.* 1999;103(12):1697-705.
14. Sylvers-Davie KL, and Davies BSJ. Regulation of lipoprotein metabolism by ANGPTL3, ANGPTL4, and ANGPTL8. *Am J Physiol Endocrinol Metab.* 2021;321(4):E493-E508.
15. Cushing EM, Chi X, Sylvers KL, Shetty SK, Potthoff MJ, and Davies BSJ. Angiopoietin-like 4 directs uptake of dietary fat away from adipose during fasting. *Mol Metab.* 2017;6(8):809-18.
16. Kersten S, Mandard S, Tan NS, Escher P, Metzger D, Chambon P, et al. Characterization of the fasting-induced adipose factor FIAF, a novel peroxisome proliferator-activated receptor target gene. *J Biol Chem.* 2000;275(37):28488-93.
17. Spitler KM, Shetty SK, Cushing EM, Sylvers-Davie KL, and Davies BSJ. Regulation of plasma triglyceride partitioning by adipose-derived ANGPTL4 in mice. *Sci Rep.* 2021;11(1):7873.
18. Ploug M. ANGPTL4: a new mode in the regulation of intravascular lipolysis. *Curr Opin Lipidol.* 2022;33(2):112-9.

19. Kersten S. Role and mechanism of the action of angiopoietin-like protein ANGPTL4 in plasma lipid metabolism. *J Lipid Res.* 2021;62:100150.
20. Dijk W, Beigneux AP, Larsson M, Bensadoun A, Young SG, and Kersten S. Angiopoietin-like 4 promotes intracellular degradation of lipoprotein lipase in adipocytes. *J Lipid Res.* 2016;57(9):1670-83.
21. Dijk W, Ruppert PMM, Oost LJ, and Kersten S. Angiopoietin-like 4 promotes the intracellular cleavage of lipoprotein lipase by PCSK3/furin in adipocytes. *J Biol Chem.* 2018;293(36):14134-45.
22. Aryal B, Singh AK, Zhang X, Varela L, Rotllan N, Goedeke L, et al. Absence of ANGPTL4 in adipose tissue improves glucose tolerance and attenuates atherogenesis. *JCI Insight.* 2018;3(6).
23. Dewey FE, Gusarova V, O'Dushlaine C, Gottesman O, Trejos J, Hunt C, et al. Inactivating Variants in ANGPTL4 and Risk of Coronary Artery Disease. *N Engl J Med.* 2016;374(12):1123-33.
24. Desai U, Lee EC, Chung K, Gao C, Gay J, Key B, et al. Lipid-lowering effects of anti-angiopoietin-like 4 antibody recapitulate the lipid phenotype found in angiopoietin-like 4 knockout mice. *Proc Natl Acad Sci U S A.* 2007;104(28):11766-71.
25. Zechner R, Zimmermann R, Eichmann TO, Kohlwein SD, Haemmerle G, Lass A, et al. FAT SIGNALS--lipases and lipolysis in lipid metabolism and signaling. *Cell metabolism.* 2012;15(3):279-91.
26. Yang X, Lu X, Lombes M, Rha GB, Chi YI, Guerin TM, et al. The G(0)/G(1) switch gene 2 regulates adipose lipolysis through association with adipose triglyceride lipase. *Cell Metab.* 2010;11(3):194-205.
27. Zhang X, Xie X, Heckmann BL, Saarinen AM, Czyzyk TA, and Liu J. Targeted disruption of g0/g1 switch gene 2 enhances adipose lipolysis, alters hepatic energy balance, and alleviates high-fat diet-induced liver steatosis. *Diabetes.* 2014;63(3):934-46.
28. Cerk IK, Salzburger B, Boeszoermenyi A, Heier C, Pillip C, Romauch M, et al. A Peptide Derived from G0/G1 Switch Gene 2 Acts as Non-competitive Inhibitor of Adipose Triglyceride Lipase. *The Journal of biological chemistry.* 2014.
29. Zhang X, Heckmann BL, Campbell LE, and Liu J. G0S2: A small giant controller of lipolysis and adipose-liver fatty acid flux. *Biochim Biophys Acta.* 2017;1862(10 Pt B):1146-54.
30. Ma T, Lopez-Aguiar AG, Li A, Lu Y, Sekula D, Nattie EE, et al. Mice lacking G0S2 are lean and cold-tolerant. *Cancer biology & therapy.* 2014;15(5).
31. El-Assaad W, El-Kouhen K, Mohammad AH, Yang J, Morita M, Gamache I, et al. Deletion of the gene encoding G0/G 1 switch protein 2 (G0s2) alleviates high-fat-diet-induced weight gain and insulin resistance, and promotes browning of white adipose tissue in mice. *Diabetologia.* 2015;58(1):149-57.
32. Heier C, Radner FP, Moustafa T, Schreiber R, Grond S, Eichmann TO, et al. G0/G1 Switch Gene 2 Regulates Cardiac Lipolysis. *The Journal of biological chemistry.* 2015;290(43):26141-50.
33. Burr SD, Chen Y, Hartley CP, Zhao X, and Liu J. Replacement of saturated fatty acids with linoleic acid in western diet attenuates atherosclerosis in a mouse model with inducible ablation of hepatic LDL receptor. *Sci Rep.* 2023;13(1):16832.

34. Ong JM, Kirchgessner TG, Schotz MC, and Kern PA. Insulin increases the synthetic rate and messenger RNA level of lipoprotein lipase in isolated rat adipocytes. *J Biol Chem.* 1988;263(26):12933-8.
35. Semenkovich CF, Wims M, Noe L, Etienne J, and Chan L. Insulin regulation of lipoprotein lipase activity in 3T3-L1 adipocytes is mediated at posttranscriptional and posttranslational levels. *J Biol Chem.* 1989;264(15):9030-8.
36. Kuo T, Chen TC, Yan S, Foo F, Ching C, McQueen A, et al. Repression of glucocorticoid-stimulated angiopoietin-like 4 gene transcription by insulin. *J Lipid Res.* 2014;55(5):919-28.
37. Yamada T, Ozaki N, Kato Y, Miura Y, and Oiso Y. Insulin downregulates angiopoietin-like protein 4 mRNA in 3T3-L1 adipocytes. *Biochem Biophys Res Commun.* 2006;347(4):1138-44.
38. Ahmadian M, Duncan RE, Varady KA, Frasson D, Hellerstein MK, Birkenfeld AL, et al. Adipose overexpression of desnutrin promotes fatty acid use and attenuates diet-induced obesity. *Diabetes.* 2009;58(4):855-66.
39. Schoiswohl G, Stefanovic-Racic M, Menke MN, Wills RC, Surlow BA, Basantani MK, et al. Impact of Reduced ATGL-Mediated Adipocyte Lipolysis on Obesity-Associated Insulin Resistance and Inflammation in Male Mice. *Endocrinology.* 2015;156(10):3610-24.
40. Schreiber R, Hofer P, Taschler U, Voshol PJ, Rechberger GN, Kotzbeck P, et al. Hypophagia and metabolic adaptations in mice with defective ATGL-mediated lipolysis cause resistance to HFD-induced obesity. *Proceedings of the National Academy of Sciences of the United States of America.* 2015;112(45):13850-5.
41. Schweiger M, Romauch M, Schreiber R, Grabner GF, Hutter S, Kotzbeck P, et al. Pharmacological inhibition of adipose triglyceride lipase corrects high-fat diet-induced insulin resistance and hepatosteatosis in mice. *Nat Commun.* 2017;8:14859.
42. Gomes D, Wang S, Goodspeed L, Turk KE, Wietecha T, Liu Y, et al. Comparison between genetic and pharmaceutical disruption of Ldlr expression for the development of atherosclerosis. *J Lipid Res.* 2022;63(3):100174.
43. Ochiai M. Evaluating the appropriate oral lipid tolerance test model for investigating plasma triglyceride elevation in mice. *PLoS One.* 2020;15(10):e0235875.
44. Brouns F, Bjorck I, Frayn KN, Gibbs AL, Lang V, Slama G, et al. Glycaemic index methodology. *Nutr Res Rev.* 2005;18(1):145-71.
45. Kraus D, Yang Q, and Kahn BB. Lipid Extraction from Mouse Feces. *Bio Protoc.* 2015;5(1).
46. Gavrilova O, Marcus-Samuels B, Graham D, Kim JK, Shulman GI, Castle AL, et al. Surgical implantation of adipose tissue reverses diabetes in lipoatrophic mice. *J Clin Invest.* 2000;105(3):271-8.
47. Rooks C, Bennet T, Bartness TJ, and Harris RB. Compensation for an increase in body fat caused by donor transplants into mice. *Am J Physiol Regul Integr Comp Physiol.* 2004;286(6):R1149-55.
48. Salazar-Olivo LA, Castro-Munozledo F, and Kuri-Harcuch W. A preadipose 3T3 cell variant highly sensitive to adipogenic factors and to human growth hormone. *J Cell Sci.* 1995;108 (Pt 5):2101-7.

49. Zhang X, Heckmann BL, and Liu J. Studying lipolysis in adipocytes by combining siRNA knockdown and adenovirus-mediated overexpression approaches. *Methods in cell biology.* 2013;116:83-105.

Figure 1

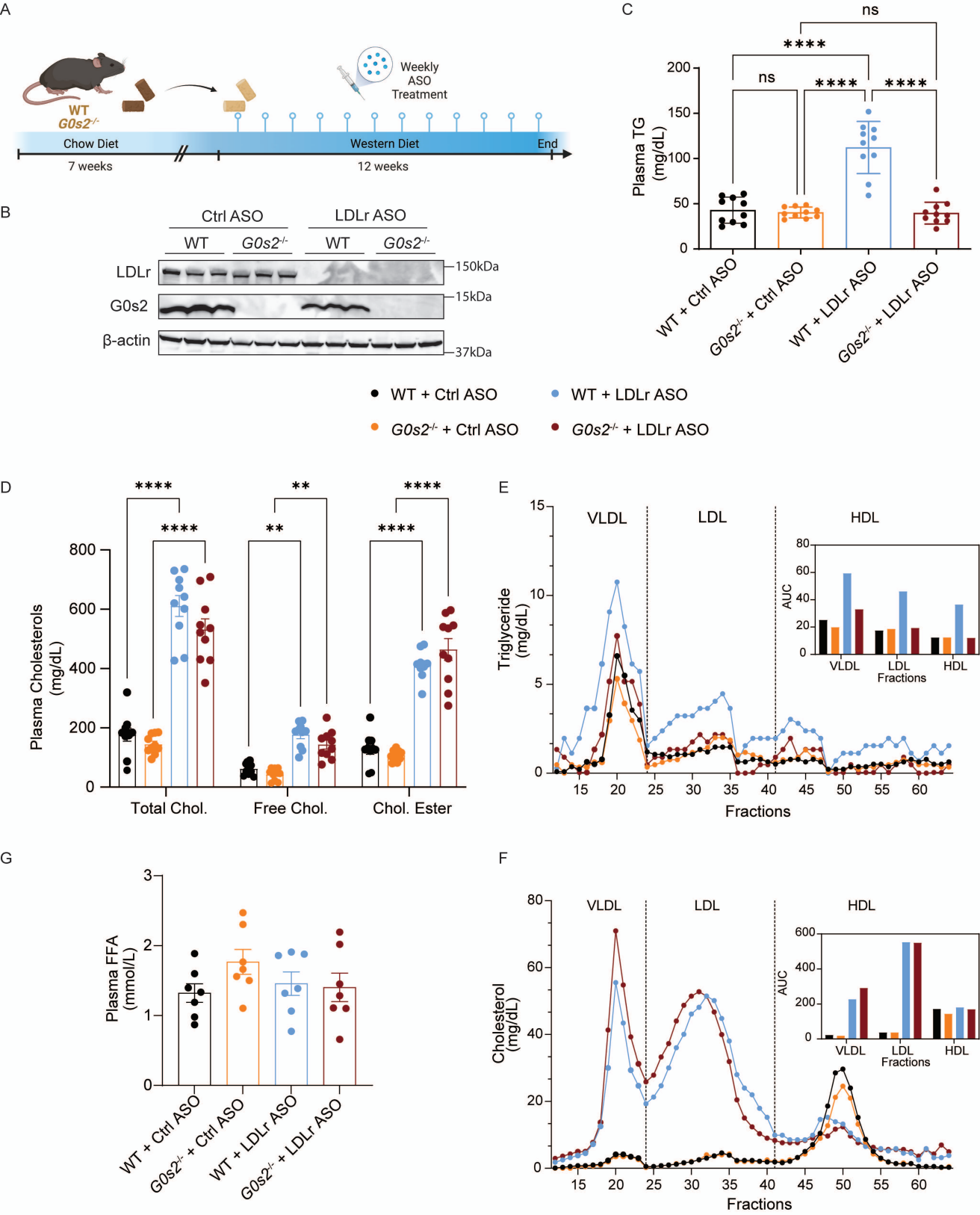
A
WT
G0s2-/-
Weekly
ASO
Treatment
Chow Diet
7 weeks
Western Diet
12 weeks
End
B
Ctrl ASO
LDLr ASO
WT
G0s2-/-
WT
G0s2-/-
LDLr
G0s2
β-actin
150kDa
15kDa
37kDa
C
ns
****
ns
****
****
Plasma TG
(mg/dL)
200
150
100
50
0
WT + Ctrl ASO
G0s2-/- + Ctrl ASO
WT + LDLr ASO
G0s2-/- + LDLr ASO
WT + Ctrl ASO
WT + LDLr ASO
G0s2-/- + Ctrl ASO
G0s2-/- + LDLr ASO
D
****
****
**
**
****
****
Plasma Cholesterols
(mg/dL)
800
600
400
200
0
Total Chol.
Free Chol.
Chol. Ester
E
VLDL
LDL
HDL
Triglyceride
(mg/dL)
15
10
5
0
AUC
80
60
40
20
0
VLDL
LDL
HDL
Fractions
15
20
25
30
35
40
45
50
55
60
Fractions
G
Plasma FFA
(mmol/L)
3
2
1
0
WT + Ctrl ASO
G0s2-/- + Ctrl ASO
WT + LDLr ASO
G0s2-/- + LDLr ASO
F
VLDL
LDL
HDL
Cholesterol
(mg/dL)
80
60
40
20
0
AUC
600
400
200
0
VLDL
LDL
HDL
Fractions
15
20
25
30
35
40
45
50
55
60
Fractions

Figure 1. *G0s2* ablation decreases plasma TG in mice treated with Ldlr ASO and Western diet. A. Mouse model building scheme. 7-week-old male WT and *G0s2*$^{-/-}$ mice were fed with a Western diet and treated with either control or Ldlr ASO weekly for 12 weeks. **B**. Western blot analysis of mouse liver for LDLR and G0S2. **C&D.** Fasting plasma levels of TG (**C**) and total cholesterol, free cholesterol, and cholesterol ester (**D**) after diet treatment (n=10). **E&F.** FPLC analysis of pooled plasma TG (**E**) and total cholesterol (**F**) (n=10) with AUC quantification (inserts). **G.** Fasting plasma free FA level (n=7). Data represent mean ± SEM. *$p < 0.05$, **$p < 0.01$, ***$p < 0.001$, ****$p < 0.0001$ by one-way (**C&G**) or two-way ANOVA (**D**).

Figure 2

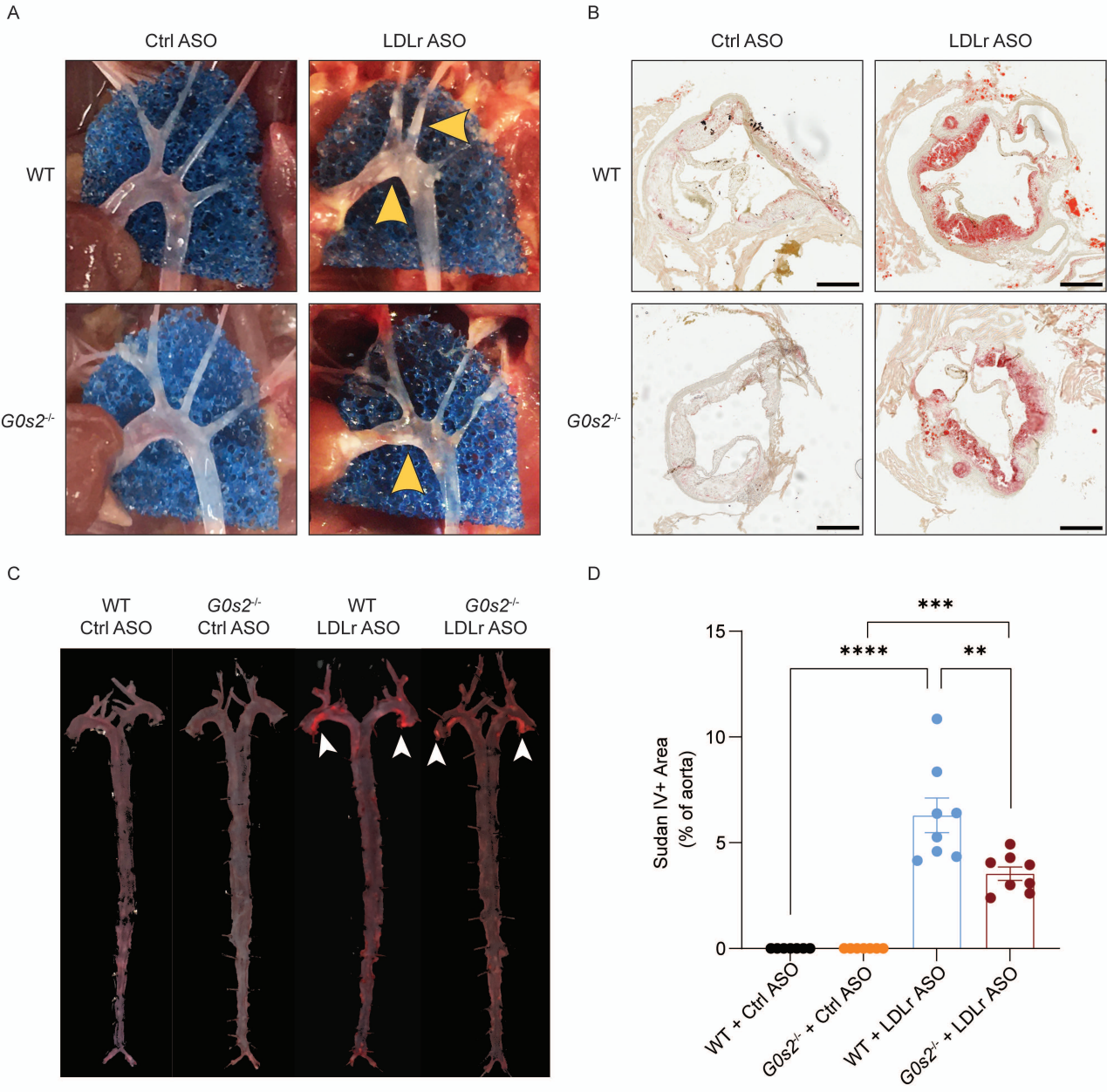
A
Ctrl ASO
LDLr ASO
WT
G0s2-/-
B
Ctrl ASO
LDLr ASO
WT
G0s2-/-
C
WT
Ctrl ASO
G0s2-/-
Ctrl ASO
WT
LDLr ASO
G0s2-/-
LDLr ASO
D
***
****
**
15
10
5
0
Sudan IV+ Area
(% of aorta)
WT + Ctrl ASO
G0s2-/- + Ctrl ASO
WT + LDLr ASO
G0s2-/- + LDLr ASO

Figure 2. *G0s2* deficiency attenuates atherosclerosis. A. Representative images depicting plaque formation (yellow arrow heads) in aortic arch. **B.** Representative images of plaques in the aortic root sections with Oil Red O staining. Scale bar=300 μm. **C.** Representative images of *en face* Sudan IV–stained aortas. **D.** Quantification of Sudan IV positive areas of total aorta (n=8). Data represent mean ± SEM. $^{**}P < 0.01$, $^{***}P < 0.001$, $^{****}P < 0.0001$ by one-way ANOVA (**D**).

Figure 3

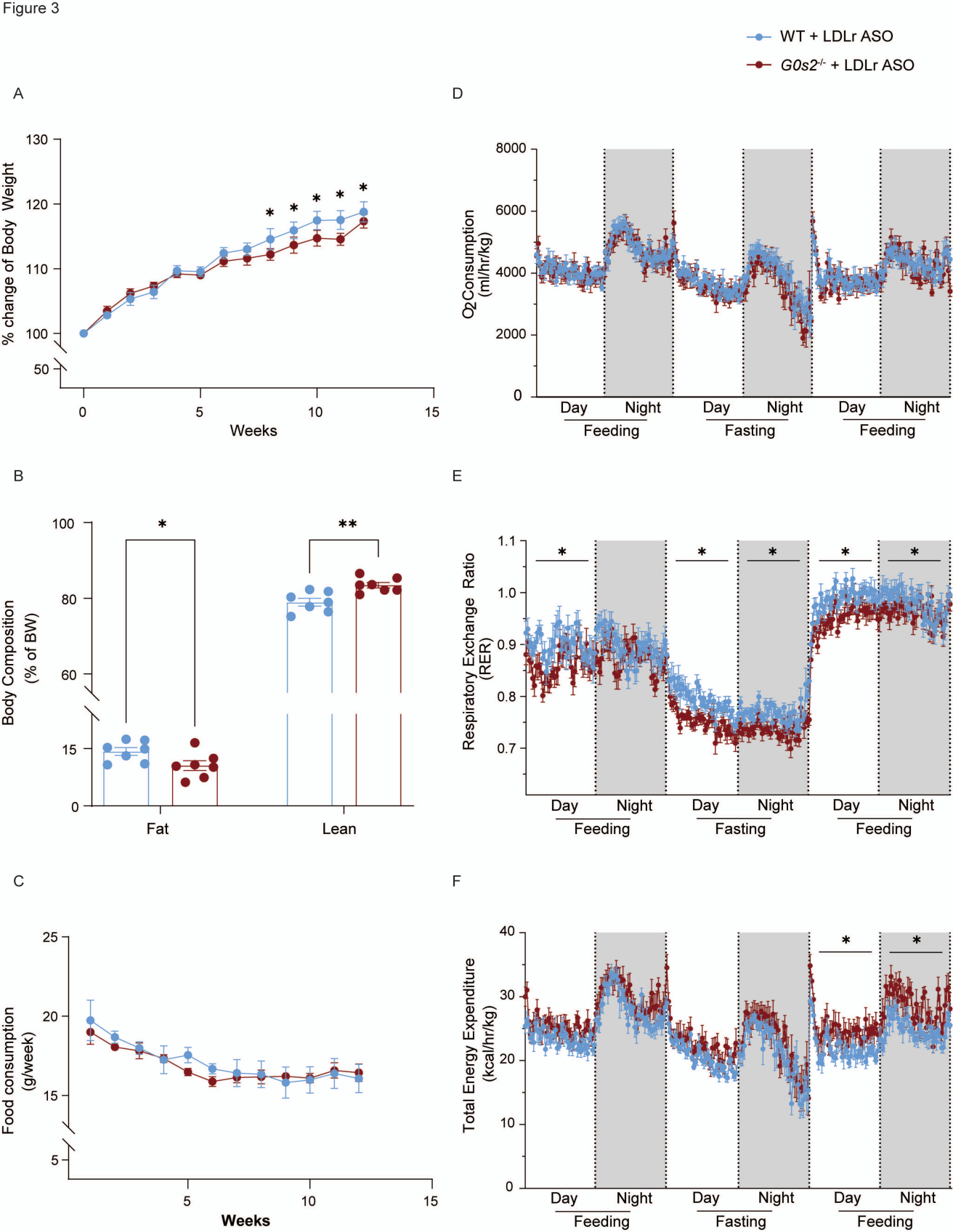
WT + LDLr ASO
G0s2-/- + LDLr ASO
A
% change of Body Weight
Weeks
B
Body Composition (% of BW)
Fat
Lean
C
Food consumption (g/week)
Weeks
D
O2Consumption (ml/hr/kg)
Day
Night
Feeding
Fasting
E
Respiratory Exchange Ratio (RER)
F
Total Energy Expenditure (kcal/hr/kg)

Figure 3. *G0s2* ablation decreases adiposity and increases whole-body lipid oxidation. A. Time course of relative body weight changes in mice treated with *Ldlr* ASO and Western diet (n=10). **B.** Body composition at the end of Ldlr ASO and diet treatment (n=7). **C.** Time course of weekly food consumption during diet treatment (n=10). **D, E&F.** Real-time curve of oxygen consumption (**D**), respiratory exchange ratio (RER) (**E**) and total energy expenditure (EE) (**F**) during feeding/fasting/refeeding cycle (n=10). Data represent mean ± SEM. *$p < 0.05$, **$p <$ 0.01by unpaired two-tailed t tests (**A, C, D, E&F**) or two-way ANOVA (**B**). Statistical analysis of metabolic cage data was performed by comparison averages of each day/night period.

Figure 4

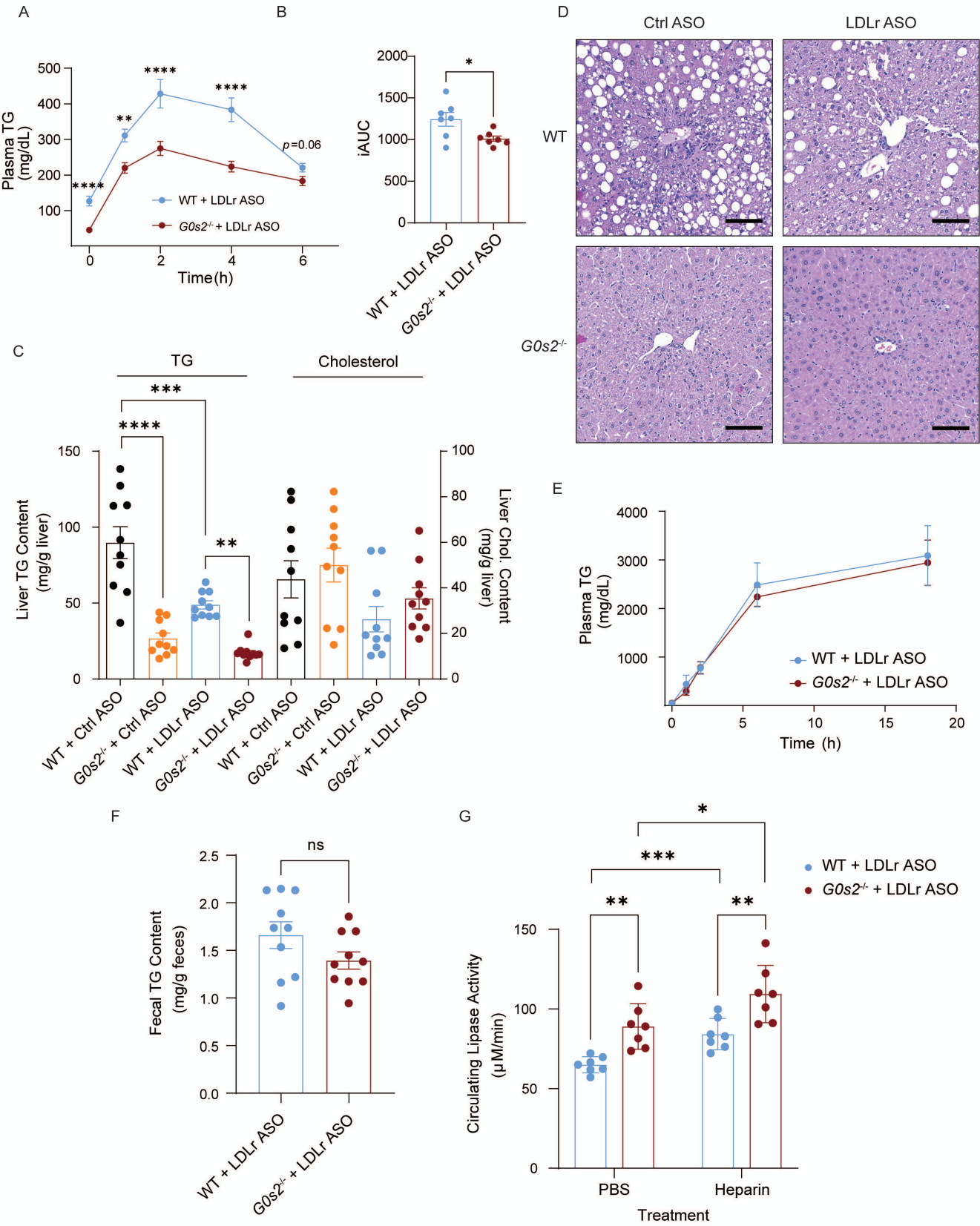
A
B
D
Ctrl ASO
LDLr ASO
WT
G0s2-/-
Plasma TG (mg/dL)
Time (h)
WT + LDLr ASO
G0s2-/- + LDLr ASO
p=0.06
iAUC
C
TG
Cholesterol
Liver TG Content (mg/g liver)
Liver Chol. Content (mg/g liver)
WT + Ctrl ASO
G0s2-/- + Ctrl ASO
WT + LDLr ASO
G0s2-/- + LDLr ASO
E
F
Fecal TG Content (mg/g feces)
ns
G
Circulating Lipase Activity (μM/min)
PBS
Heparin
Treatment

Figure 4. *G0s2* ablation improves whole-body TG clearance without affecting hepatic TG secretion in mice treated with ASO and Western diet. **A.** Time course of plasma TG levels during oral lipid tolerance test (OLTT) (n=10). **B.** iAUC analysis of OLTT plasma TG curve (n=10). **C.** Hepatic TG and cholesterol contents (n=10). **D.** Representative images of liver sections with H&E staining. Scale bar=100 μm. **E.** Hepatic TG secretion assay after P-407 administration(n=6). **F.** Fecal TG contents (n=10). **G.** Circulating LPL activity 10 mins after PBS or heparin administration, as determined following a 15-min reaction of plasma with an artificial substrate (detailed in the Materials and Methods). Data represent mean ± SEM. *$p <$ 0.05, **$p < 0.01$, ***$p < 0.001$, ****$p < 0.0001$ by unpaired two-tailed t tests (**A, B, E&F**) or two-way ANOVA (**C&G**).

Figure 5

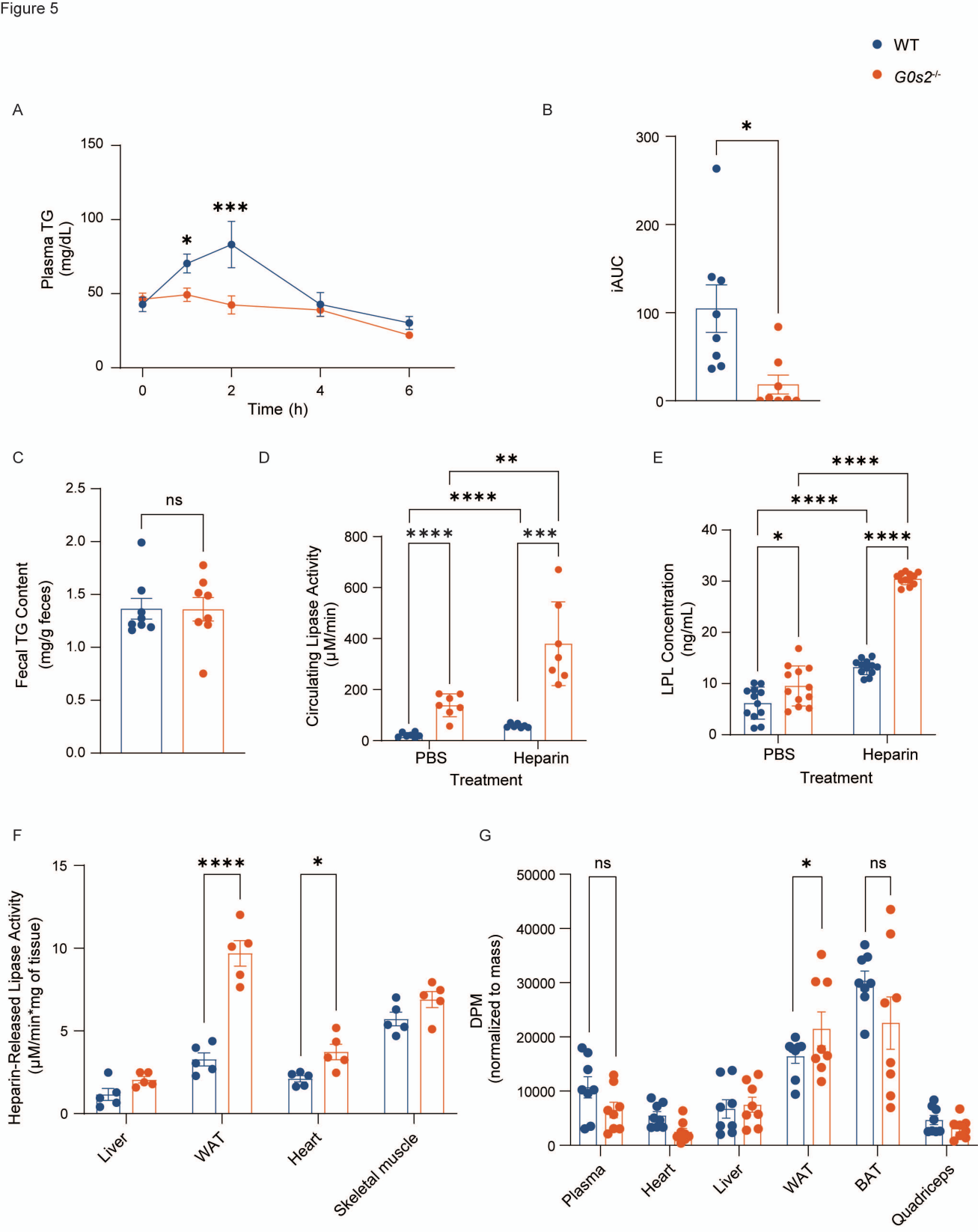
WT
G0s2-/-
A
Plasma TG (mg/dL)
Time (h)
B
iAUC
C
Fecal TG Content (mg/g feces)
ns
D
Circulating Lipase Activity (μM/min)
PBS
Heparin
Treatment
E
LPL Concentration (ng/mL)
PBS
Heparin
Treatment
F
Heparin-Released Lipase Activity (μM/min*mg of tissue)
Liver
WAT
Heart
Skeletal muscle
G
DPM (normalized to mass)
Plasma
Heart
Liver
WAT
BAT
Quadriceps

Figure 5. *G0s2* ablation increases oral lipid tolerance and LPL production in chow-fed mice. A. Time course of plasma TG levels during oral lipid tolerance test (OLTT) (n=8). **B.** iAUC analysis of OLTT plasma TG curve (n=8). **C.** Fecal TG contents (n=8). **D.** Circulating lipase activity 10 min after PBS or heparin administration, as determined following a 60-min reaction of plasma with the artificial substrate. **E.** Circulating LPL protein concentration 10 mins after PBS or heparin administration (n=11). **F.** Tissue specific LPL activity (n=5). **G.** Tissue distribution of ^{3}H radioactivity in mice 2h after oral gavage of ^{3}H-labeled triolein (n=15). Data represent mean ± SEM. *$p < 0.05$, **$p < 0.01$, ***$p < 0.001$, ****$p < 0.0001$ by unpaired two-tailed t tests (**A, B&C**) or two-way ANOVA (**D, E, F&G**).

Figure 6

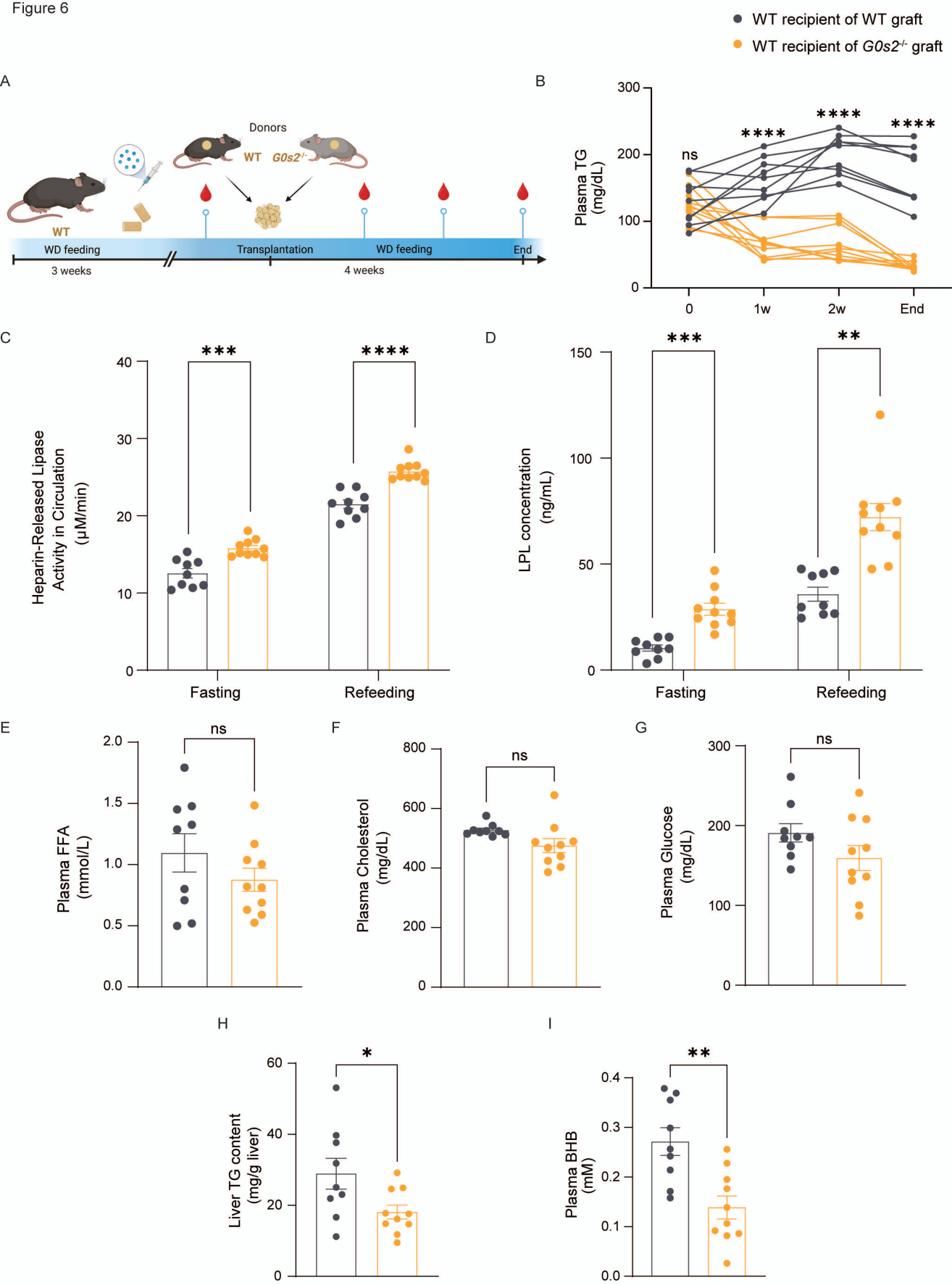
WT recipient of WT graft
WT recipient of G0s2-/- graft
A
Donors
WT
G0s2-/-
WT
WD feeding
3 weeks
Transplantation
WD feeding
4 weeks
End
B
Plasma TG (mg/dL)
ns
****
****
****
0
1w
2w
End
C
Heparin-Released Lipase Activity in Circulation (μM/min)
***
****
Fasting
Refeeding
D
LPL concentration (ng/mL)
***
**
Fasting
Refeeding
E
Plasma FFA (mmol/L)
ns
F
Plasma Cholesterol (mg/dL)
ns
G
Plasma Glucose (mg/dL)
ns
H
Liver TG content (mg/g liver)
*
I
Plasma BHB (mM)
**

Figure 6. **Transplantation with *G0s2*$^{-/-}$ WAT alleviates hypertriglyceridemia in WT recipient mice.** **A**. Experimental scheme: after 3 weeks of treatment with Western diet and Ldlr ASO, WT recipient mice were transplanted *in situ* with epididymal WAT dissected from chow-fed WT or *G0s2*$^{-/-}$ donor mice. **B**. Plasma TG concentrations prior to and after transplantation at indicated time points(n=9-10). **C&D**. Circulating lipase activity 10 min after heparin administration, as determined following a 15-min reaction of plasma with the artificial substrate (C), and LPL protein concentration (D) during fasting or refeeding 4 weeks after transplantation (n=9-10). **E-G.** Fasting plasma levels or free FA (E), total cholesterol (F), and glucose (G) at the endpoint (n=9-10). **H**. Liver TG content normalized to liver weight at the endpoint (n=9-10). **I.** Fasting plasma β-hydroxybutyrate (BHB) levels (n=9-10). Data represent mean ± SEM. *$p < 0.05$, **$p < 0.01$, ***$p < 0.001$, ****$p < 0.0001$ by unpaired two-tailed t tests (**B, E, F, G, H&I**) or two-way ANOVA (**C&D**).

Figure 7

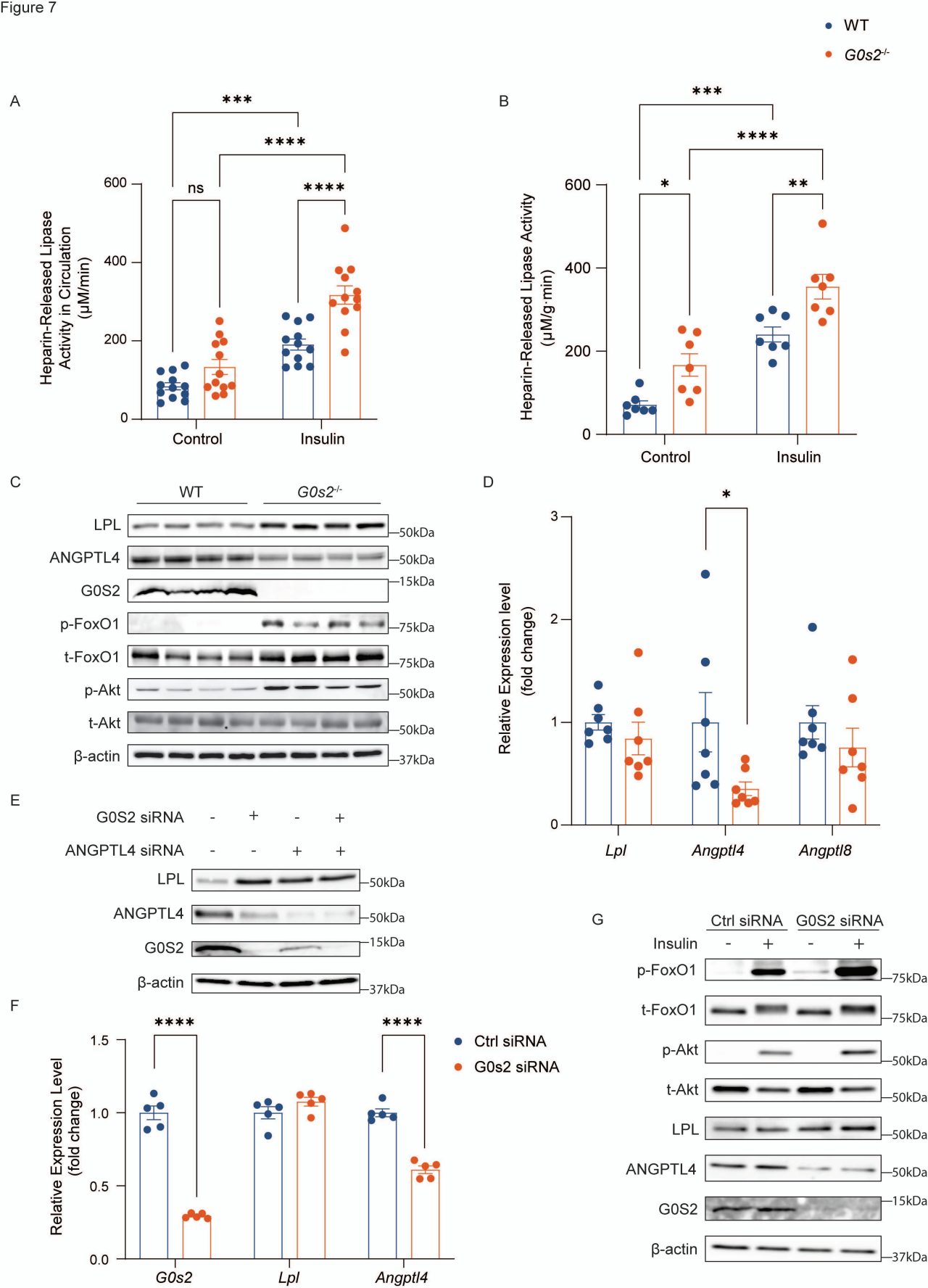
WT
G0s2-/-
A
***
****
ns
****
Heparin-Released Lipase Activity in Circulation (μM/min)
600
400
200
0
Control
Insulin
B
***
****
*
**
Heparin-Released Lipase Activity (μM/g·min)
600
400
200
0
Control
Insulin
C
WT
G0s2-/-
LPL
ANGPTL4
G0S2
p-FoxO1
t-FoxO1
p-Akt
t-Akt
β-actin
50kDa
50kDa
15kDa
75kDa
75kDa
50kDa
50kDa
37kDa
D
*
Relative Expression level (fold change)
3
2
1
0
Lpl
Angptl4
Angptl8
E
G0S2 siRNA - + - +
ANGPTL4 siRNA - - + +
LPL
ANGPTL4
G0S2
β-actin
50kDa
50kDa
15kDa
37kDa
F
****
****
Relative Expression Level (fold change)
1.5
1.0
0.5
0.0
G0s2
Lpl
Angptl4
Ctrl siRNA
G0s2 siRNA
G
Ctrl siRNA
G0S2 siRNA
Insulin - + - +
p-FoxO1
t-FoxO1
p-Akt
t-Akt
LPL
ANGPTL4
G0S2
β-actin
75kDa
75kDa
50kDa
50kDa
50kDa
50kDa
15kDa
37kDa

Figure 7. ***G0s2*** **ablation causes opposite changes in LPL and ANGPTL4 expression while increasing insulin sensitivity in adipocytes. A.** Circulating post-heparin lipase activity in chow-fed mice pre- and 1h post-insulin stimulation (n=12), **B**. Post-heparin lipase activity in the media of WAT explants without or with insulin stimulation for 45 min (n=7). In both (A) and (B), lipase activity was determined following a 60-min reaction of plasma with the artificial substrate. **C.** Western blotting analysis of proteins in epididymal WAT after 4-h refeeding. **D.** qPCR analysis of relative mRNA expression in epididymal WAT after 4-h refeeding (n=7). **E.** Western blotting analysis of 3T3-F442A adipocytes transfected with either control, G0S2-specific and/or ANGPTL4-siRNA. **F.** qPCR analysis of mRNA expression in transfected 3T3-F442A adipocytes. **G.** Western blotting analysis of transfected 3T3-F442A adipocytes after treatment with or without 100 nM of insulin for 15 min. Data represent mean ± SEM. *$p < 0.05$, **$p < 0.01$, ***$p < 0.001$, ****$p < 0.0001$ by two-way ANOVA (**A, B, D&F**). All cell experiments were conducted three times with similar results and a representative image is shown.

Figure 8

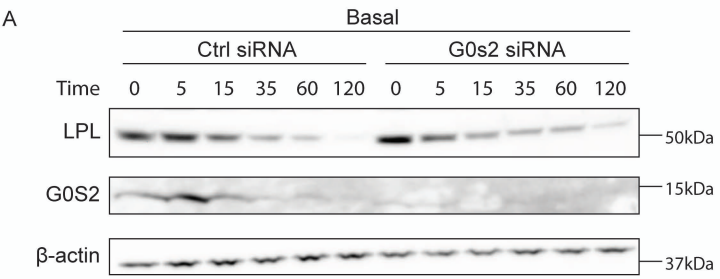
A
Basal
Ctrl siRNA
G0s2 siRNA
Time 0 5 15 35 60 120 0 5 15 35 60 120
LPL
G0S2
β-actin
50kDa
15kDa
37kDa

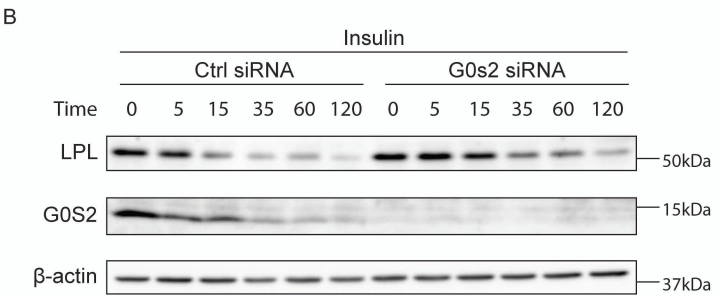
B
Insulin
Ctrl siRNA
G0s2 siRNA
Time 0 5 15 35 60 120 0 5 15 35 60 120
LPL
G0S2
β-actin
50kDa
15kDa
37kDa

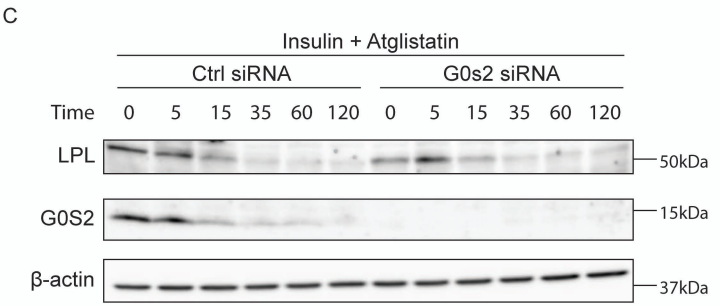
C
Insulin + Atglistatin
Ctrl siRNA
G0s2 siRNA
Time 0 5 15 35 60 120 0 5 15 35 60 120
LPL
G0S2
β-actin
50kDa
15kDa
37kDa

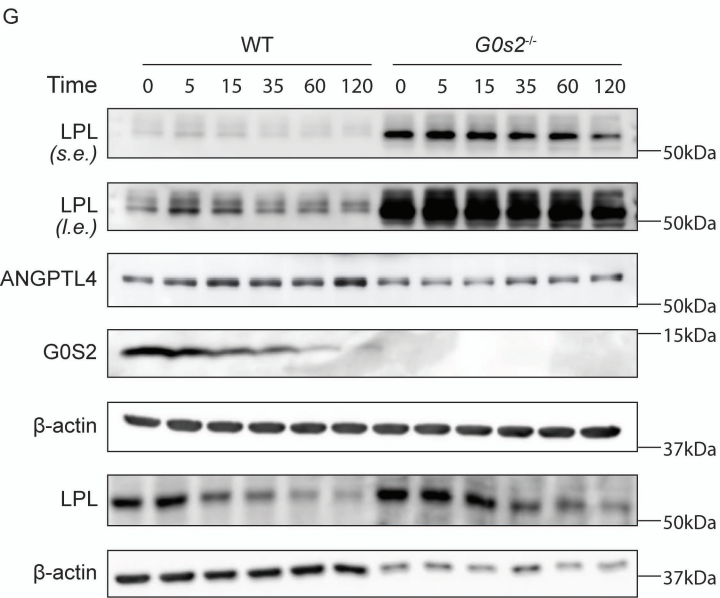
G
WT
G0s2-/-
Time 0 5 15 35 60 120 0 5 15 35 60 120
LPL (s.e.)
LPL (l.e.)
ANGPTL4
G0S2
β-actin
LPL
β-actin
50kDa
15kDa
37kDa
Normalized Loading At Time 0

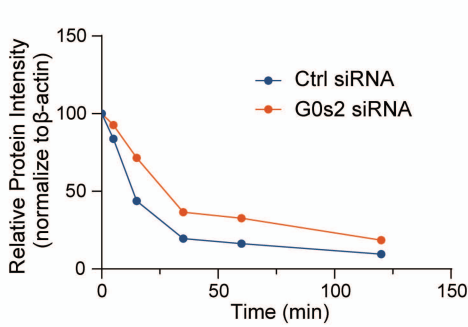
D
Relative Protein Intensity (normalize to β-actin)
Time (min)
Ctrl siRNA
G0s2 siRNA
0
50
100
150

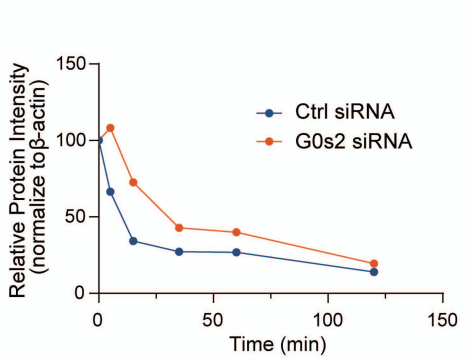
E
Relative Protein Intensity (normalize to β-actin)
Time (min)
Ctrl siRNA
G0s2 siRNA
0
50
100
150

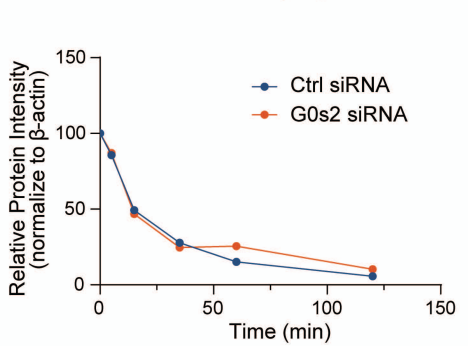
F
Relative Protein Intensity (normalize to β-actin)
Time (min)
Ctrl siRNA
G0s2 siRNA
0
50
100
150

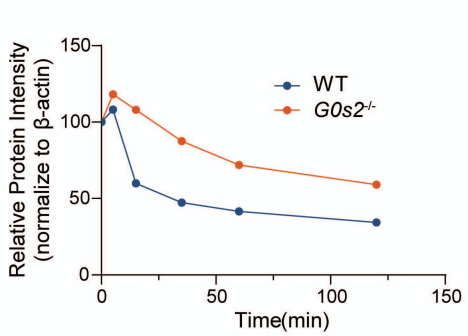
H
Relative Protein Intensity (normalize to β-actin)
Time(min)
WT
G0s2-/-
0
50
100
150

Figure 8. **Absence of *G0s2* increases LPL protein stability in adipocytes. A-C.** Western blotting analysis of protein expression in 3T3-F442A adipocytes transfected with either control or G0S2-specific siRNA and then treated with CHX in the presence of vehicle alone (**A**), 100 nM insulin (**B**) or 100 nM insulin + 10 μM Atglistatin (**C**) for the indicated time points. **D-F**. Relative quantification of LPL protein levels in panel **A** (**D**), **B** (**E**) and **C** (**F**). **G**. Western blotting analysis of SVF-derived adipocytes treated with CHX for indicated periods (*s.e.* short exposure, *l.e.* long exposure). **H.** Relative quantification of LPL intensity in panel **G**. All cell experiments were conducted three times with similar results and a representative image is shown.